Universidade de Aveiro Departamento de Eng.ª Cerâmica e do Vidro
Ano 2011

Basam Abobaker
Emhemed Ben-Arfa

Biovidros de diópsido – pirofosfato de cálcio dopados com alguns aditivos

Diopside-calcium pyrophosphate bioglasses doped with some additives

Universidade de Aveiro Departamento de Eng.ª Cerâmica e do Vidro
Ano 2011

Basam Abobaker Emhemed Ben-Arfa

Biovidros de diópsido – pirofosfato de cálcio dopados com alguns aditivos

Diopside-calcium pyrophosphate bioglasses doped with some additives

Dissertação apresentada à Universidade de Aveiro para cumprimento dos requisitos necessários à obtenção do grau de Mestre em Materiais e dispositivos biomédicos, realizada sob a orientação científica do Prof. Doutor José Maria Ferreira, e do Dr. Ashutosh Goel, Departamento de Engenharia Cerâmica e do Vidro, CICECO, Universidade de Aveiro.

Thesis submitted to University of Aveiro for fulfillment of the requirements for the degree of Master in Biomedical Materials and device held under the scientific guidance of Professor Dr. José Maria Ferreira and Dr. Ashutosh Goel, Department of Ceramics and Glass Engineering, CICECO, University of Aveiro.

Dedico este trabalho à memória do meu pai, à minha mãe, à minha mulher e aos meus filhos.

Dedicated to the soul of my father, and to my mother, my wife and my children.

o júri

presidente	Professora Doutora Maria Elisabete Jorge Vieira da Costa professora do departamento de Eng.ª Cerâmica e do Vidro da Universidade de Aveiro
arguente	Professora Doutora Maria Clara Henriques Baptista Gonçalves professora auxiliar do departamento de Eng.ª Química da Universidade Técnica de Lisboa
orientador	Professor Doutor José Maria da Fonte Ferreira professor do departamento de Eng.ª Cerâmica e do Vidro da Universidade de Aveiro

Acknowledgements

First and foremost, I would like to acknowledge the following individuals for providing me with the inspiration to embark on my MSc. candidature. My deepest thanks go to the coordinator of our master course; Prof[a]. Dr[a] M. Helena Fernandes for her help and advice during my Master program.

I would like to convey my gratitude to my supervisors who shepherded during the circumstances I passed by; my associate supervisor Prof. Dr. José Maria da Fonte Ferreira, and Dr. Ashutosh Goel for their help and precious advice. Their detailed and constructive comments were vital to the development of this thesis. Their dynamic guidance at all stages of work encouraged me to accomplish my work successfully.

I would like to convey my gratitude for all of the professors who teach me during my master program, and all the auxiliary staff in the department of ceramic and glass engineering.

I would like to express my gratefulness and thanks to all of my colleagues, Hugo Fernandes, Raghu Raman Rajagopal, Allu Amarnath Reddy; people who provided technical support and assistance during the run of the experiments.

palavras-chave Vidros, vitrocerâmicos, biomateriais, sinterização, cristalização.

resumo

O objectivo do presente trabalho é o de mostrar a influência de vários iões funcionais (Y^{3+}, Cu^{2+}, F^{1-}, Mn^{2+} e Ti^{4+}) na capacidade de formação de vidro, na sua estrutura, aptidão para serem sinterizados, no comportamento na cristalização e nas várias propriedades termofísicas de vidros e vitro-cerâmicos obtidos a partir de um vidro base formulado no sistema diópsido – pirofosfato de cálcio.

Ao vidro base foram adicionadas três quantidades diferentes de cinco compostos dopantes de modo a obter cinco séries de vidros por fusão. A análise estrutural dos vidros foi feita por ressonância magnética nuclear (NMR) dos elementos ^{29}Si e ^{31}P e por espectroscopia de infravermelho associada a transformas de Fourier (FTIR). A rede de silicato em todos os vidros investigados encontra-se predominantemente coordenada em unidades Q^2 (Si), enquanto o fósforo tende a permanecer no seu ambiente de ortofosfato (Q^0). Todos os vidros apresentaram taxas rápidas de biomineralização, tornando-os bons candidatos para aplicações biomédicas.

Os comportamentos dos pós de vidro na sinterização e na cristalização foram estudados por análise termal diferencial (DTA), enquanto a dilatometria foi usada para determinar os valores do coeficiente de expansão térmica de todos os vidros. A evolução das fases cristalinas e a microestrutura dos vitro-cerâmicos foram analisadas por difracção de raio x (XRD) e por microscopia de electrónica de varrimento (SEM). Os vitro-cerâmicos foram obtidos por sinterização e cristalização dos pós dos vidros respectivos por tratamento térmico a 800, 850, e 900 °C durante 1 h.

keywords glass, glass ceramics, biomaterial, sintering, crystallisation.

abstract

The aim of the present work is to show the influence of various functional ions (Y^{3+}, Cu^{2+}, F^{1-}, Mn^{2+} and Ti^{4+}) on the glass forming ability, structure, sintering ability, crystallization behaviour and various thermo-physical properties of glasses and glass-ceramics in the diopside–calcium pyrophosphate system.

Five series of glasses have been prepared by melt-quenching technique, by doping the parent glass with 3 different percentages for each doping additive. The structural analysis of glasses has been made by ^{29}Si and ^{31}P-nuclear magnetic resonance (NMR) and Fourier transforms infrared spectroscopy (FTIR). The silicate network in all the investigated glasses is predominantly coordinated in Q^2 (Si) units while phosphorus tends to remain in orthophosphate (Q^0) environment. All glasses exhibited fast biomineralization rates, making them promising candidates for biomedical applications.

The sintering and crystallization behaviours of glass powders were studie by differential thermal analysis (DTA), while dilatometry was used to get the results about the coefficient of thermal expansion for all glasses. Crystalline phase evolution and microstructure of glass-ceramics has been followed by X-ray diffraction (XRD) and scanning electron microscopy (SEM). Glass ceramics were obtained by sintering and crystallization of glass powder compacts from all the glasses at 800,850 and 900 ºC for 1 h.

List of Tables

List of figures

Abbreviations

- Si^{4+} - Silicon ion
- Ca^{2+} - Calcium ion
- P^{5+} - Phosphorus ion
- Mg^{2+} - Magnesium ion
- F^{1-} - Ftouride ion
- Cu^{2+} - Copper ion
- Mn^{2+} - Manganese ion
- Y^{3+} - Yttrium ion
- Ti^{4+} - Titanium ion
- Di - Diopside
- CaPP - Calcium pyrophosphate
- Pt - Platinum crucibles
- KBr - Potassium bromide
- SBF - Simulated body fluid
- GC - Glass ceramic
- BO - Bridging oxygen
- ppm - Parts per million
- CTE - Coefficient of thermal expansion
- T_g - Glass transition temperature
- T_c - Onset temperature of crystallization
- HA - Hydroxyapatite
- S - Silicate
- C - Calcite
- CaP - Calcium phosphate
- CO_3^{2-} - Carbonate
- SD - Supersaturation degree
- A - Amorphous
- YO - Yttrium Oxide
- FA - Fluorapatite

Contents

Chapter 1
State of the art

1. State of the art

1.1 Introduction

The development of first generation bio-inert materials in the 1960s and 1970s for application in human body laid the foundation stone in the field of biomaterials. Since then, a tremendous advancement has been made in this research area, which has led to the development of second generation bioactive materials during 1980s. Bioactive materials have the ability to bond to bone tissue through the formation of hydroxyapatite layer on their surface via a series of controlled reactions in the physiological environment [1]. In today's era, third generation biomaterials are being designed to stimulate specific cellular responses at the molecular level [2]. While the second generation of biomaterials was designed to be either resorbable or bioactive, the third generation biomaterials is combining these two properties, with the aim of developing materials that once implanted, will help the body heal itself [3]. Bioactive glasses and glass-ceramics are typical examples of third generation biomaterials as they have the ability to exhibit surface reactivity when in contact with body fluids leading to the release of ionic dissolution products (example: Si^{4+}, Ca^{2+}, P^{5+}, Mg^{2+}, F^{1-}), which further stimulate the various vital mechanisms in human body like gene expression, osteoblast proliferation, angiogenesis and also provide anti-bacterial as well as anti-inflammatory effects [2-6]. There has been increasing evidence in the literature that ionic dissolution products from inorganic materials are the key to understand the behaviour of these materials in vitro and in vivo, in the context of tissue engineering applications [7].

Since the role of major functional ions (Ca^{2+}, Mg^{2+}, Si^{4+}, P^{5+}) in bone regeneration and soft tissue engineering has been well established and documented [2, 6, 8, 9], the focus of research is shifting towards exploring the role of different functional ions that although being present in trace quantities in human body, are essential for good metabolism. For example: zinc is an essential trace element which plays a vital role in bone formation, resorption and tissue engineering as it directly activates aminoacyl-tRNA synthetase (a rate-limiting enzyme at translational process of protein synthesis) in osteoblastic cells and stimulates cellular protein synthesis [10]. Also zinc has been shown to stimulate gene expression of the transcription factors: runt-related transcription factor 2 (Runx2) that is related to differentiation into osteoblastic cells. Moreover, zinc inhibits osteoclastic bone resorption by inhibiting osteoclast-like cell formation from bone marrow cells and

stimulating apoptotic cell death of mature osteoclasts [10]. Similarly, other ions like yttrium, copper and fluoride are being incorporated in small quantities to biomaterials in order to enhance the cellular response and stimulate gene expressions through dissolution of these ions into body fluids *in vivo* [11-13].

Our work is aimed at investigating influence of different functional ions (Cu^{2+}, Mn^{2+}, Y^{3+}, $F1^{-}$, Ti^{4+}) on structure, thermal behaviour and in vitro apatite forming ability of phosphosilicate based bioactive glasses. This study is scientifically relevant owing to the fact that the structure of glasses plays a crucial role in deciding their bioactivity [14]. Because of that, several literature reports [15-21]attempted to document the influence of the most commonly used functional ions present in the bioactive glasses (i.e. Ca^{2+}, Mg^{2+}, Si^{4+}, P^{5+}) on their structure and bioactivity. However, literature survey reveals that almost negligible amount of data has been reported on the structure-property relationships in bioactive glasses with respect to the influence of various functional ions. Therefore, this study is an attempt to fill in the existing lacuna.

1.2 Design of glass compositions

The parent glass composition has been chosen in the diopside ($CaMgSi_2O_6$; hereafter referred as Di) - calcium pyrophosphate ($Ca_2P_2O_7$; hereafter referred as CaPP) binary system with the ratio of Di/CaPP = 90/10 (wt. %). The choice of Di-CaPP binary system was made owing to the fact that the structure of amorphous Di glass is dominated by Q^2 (Si) species [22], which is an important and positive attribute, as it is well known that the highest bioactivity from a phospho-silicate glass can be expected if Q^n (Si) units (n: number of bridging oxygens) are dominated by chains of Q^2 metasilicates, which are occasionally cross-linked through Q^3 units, whereas Q^1 units terminate the chains [14]. Further, Di is known to exhibit good sintering behaviour, thus resulting in mechanically strong bioactive materials [23]. However, the major drawback of Di-based glasses and glass-ceramics is their low dissolution rate [24], which could be controlled by adding/substituting some bioresorbable material (for example: CaPP) in the final product. Therefore, the addition of CaPP at the expenses of Di in the glass compositions is expected to enhance their solubility as well as their bioactivity in physiological fluids. Also, the phosphate component in these glasses has been intentionally kept lower because if P_2O_5 in the glass is lower than 10 mol.%, the resulting phosphate species in bioactive glass can

coordinate themselves in orthophosphate environment (Q^0), thus enhancing the bioactivity of glass [21]. The parent glass will be doped with 1, 3, and 5 wt. % of different oxides, and calcium fluoride according to the table 1

Table 1 shows the different wt. % of the additives and their designations.

Wt%	Y_2O_3	CuO	MnO	CaF_2	TiO_2
1	Y-1	Cu-1	Mn-1	F-1	Ti-1
3	Y-3	Cu-3	Mn-3	F-3	Ti-3
5	Y-5	Cu-5	Mn-5	F-5	Ti-5

With respect to the choice and amount of functional ions to be incorporated in the bioactive glasses, there selection was made on the basis of their biological role in various cellular activities in human body as described below:

(i) ***Yttrium:*** Yttrium is known to enhance the mechanical properties of ceramics and promotes osteoblast adhesion. Webster et al. [25] investigated the osteoblast adhesion on hydroxyapatite doped with either cadmium (Cd), Zinc (Zn), magnesium (Mg) or yttrium (Y). They observed that osteoblast adhesion was significantly greater for Y-containing hydroxyapatite in comparison to samples doped with other ions. Similar results have also been reported by Sato et al. [26]. Also, it has been demonstrated that the presence of yttrium in biomaterials increases their electrical conductivity [27] which is presumably beneficial for bone regeneration and orthopaedic implants as cell proliferation has been shown to be sensitive to electrical currents [28]. Although, the optimum concentration level of yttrium for promoting osteoblast differentiation and proliferation is still ambiguous, however, the beneficial aspects of this element have been reported to be dose-dependent [29]. Yttrium containing bioactive glasses are not only in demand for their enhancing effect on osteoblast proliferation, but they are also potential candidates for a new generation of radionuclide vectors for cancer therapy, with high biocompatibility and controlled biodegradability [30]. However, a very delicate balance must be struck in this case as the glass compositions suitable for radiotherapy application should be stable enough to avoid releasing any radioactive yttrium into the blood stream in the initial stages of treatment, while at the same time maintaining its unique surface reactivity and ability to interact with biological

host. The structure of glasses plays a crucial role in deciding their ion release behaviour; especially the release of yttrium ion from glass in aqueous medium is controlled by its coordination environment and its clustering behaviour. Therefore, it becomes mandatory to study the influence of yttrium on the structure of bioactive glasses in order to understand the correlation between molecular structure and chemical durability of glasses as a function of yttrium content.

(ii) ***Fluoride:*** Fluoride is well known to prevent dental decay by inhibiting enamel and dentine demineralization, enhancement of demineralization and inhibition of bacterial enzymes. Also, it is a well-documented as anticarcinogenic agent. In a number of studies reduced caries experience has been attributed to elevated salivary fluoride levels. It has been stated that a constant supply of low levels of intraoral fluoride is of most benefit in preventing caries. An elevation of the fluoride level in saliva from 0.001 to 0.005–0.010 $mmolL^{-1}$, e.g. 5–10 times, for prolonged periods may be efficient for caries control [31]. Fluoride is also known to increase bone density and despite some dispute on dose and effectiveness in prevention of fractures, it is of interest for treatment of osteoporosis [32, 33]. According to Pak et al. [34], fluoride exerts a biphasic action at the level of osteoblasts, on bone mineral, on bone structure and function, and in treatment of osteoporosis. At low circulating concentrations ($\leq$ 500 ng mL^{-1}), skeletal uptake of fluoride is limited and the effects are beneficial (stimulate osteoblasts proliferation) while at higher concentrations and greater skeletal uptake, fluoride may cause osteoblast suppression leading to the formation of abnormally mineralized bone of impaired quality. These results have also been verified by clinical trials on human patients during treatment of spinal fractures [34]. This limits the fluoride content in bioactive glasses to low amounts.

(iii) ***Copper:*** Copper containing phosphate glasses with antimicrobial activity were prepared by Mulligan et al. [13] for potential applications in the treatment of oral infections. The aim was to develop glass devices that could be placed at the site of an infection such as in a periodontal pocket to treat the infection with the antimicrobial ions released as the glass degrades. Mulligan et al. [13] study has

been focused on glass systems with a fixed P_2O_5 concentration of 45 mol%, and concentrations of the antibacterial ions, Cu^{2+} or Ag^{+}, of 0, 1, 5, 10 and 15 mol%. Apart from that, copper is known to play an essential role in angiogenesis as significant amount of Cu is found in human endothelial cells when undergoing angiogenesis. In a recent study by Gerard et al. [35], the synergistic stimulating effect of copper ions on angiogenesis in combination with two major angiogenic factors (FGF-2 and VEGF) has been demonstrated. In another study by Dahl et al. [36], it has been shown that a gradual increase in copper ion concentration in culture medium enhanced the growth of engineered arterial tissue while low copper concentration or a sudden increase in copper ion concentration in culture media retarded the tissue growth. This shows that a gradual and controlled release of ions in culture media is required for the optimal cell proliferation. Even more, copper plays important functional roles in bone metabolism and turnover. It is known that it is essential for normal growth and development of the skeleton in humans and in animals. Although at present, the exact role that copper plays in bone metabolism is unknown, bone abnormalities are a feature of severe copper deficiency [37].

(iv) ***Manganese:*** The motivation for addition of Mn is due to good biological properties. The biologically important metal manganese is an essential key cofactor for metalloenzymes (oxidases and dehydrogenases), DNA polymerases and kinases [38]. Furthermore, this divalent cation is known to strongly influence the integrin avidity and the integrin affinity to ligands and – in consequence – cell adhesion to extracellular matrix proteins [39]. Mn influences regulation of bone remodelling, and its deficit causes reduction of organic matrix synthesis and retards endochondral osteogenesis, increasing the possibility of bone abnormalities such as decrease of bone thickness or length [40]. Mn supplement was found to be an effective inhibitor of loss of bone mass after ovariectomy [41]. Luthen et al. [42] investigated the influence of manganese ions on cellular functions like spreading, proliferation and gene expression in human osteoblasts. They suggested that the effect of Mn cations on cell functions is strongly concentration dependent as higher Mn concentration resulted in reduced spreading, proliferation as well as phosphorylation of signalling proteins. While the deficiency of manganese may

result in the delayed osteogenesis process due to lower activity of osteoblasts. This may lead to bone deformation, growth inhibition, and even to bone resorption [43].This justifies the lower concentration of these elements used in the present study.

(v) ***Titanium:*** Owing to the bioinert nature of Ti, its alloys are frequently used for dental and orthopaedic implants because of low toxicity, superior corrosion resistance, favourable mechanical properties and good biocompatibility [44]. However, incorporating Ti in biomaterials has been shown to enhance their biological activity. For example: Vrouwenvelder et al. [45] reported on the osteoblast behaviour on 45S5 Bioglass® doped with iron, titanium, fluorine and boron. It was shown that Ti-containing bioactive glass exhibited higher proliferation and osteoblast expression whereas doping with B, Fe and F resulted in lower osteoblast activity compared to undoped control 45S5 Bioglass®. Similarly, in a study on Ti-containing phosphate based biactive glasses by Abou Neel et al. [46], it has been shown that addition of TiO_2 in small amounts (up to 5 mol.%) enhances biocompatibility of these glasses in vitro as well as in vivo.

"With the above mentioned perspective, 1, 3 and 5 wt. % of additives (CuO, MnO, Y_2O_3, CaF_2 and TiO_2, respectively) were added to the parent glass composition. The compositions of all the investigated glasses have been presented in Table 2.1 (wt. %) and Table 2.2 (mol. %)".

Chapter 2
Experimental Procedure

2. Experimental Procedures

2.1 Glasses Synthesis

Tables 2.1 and 2.2 present the detailed compositions of glasses investigated in the present study in wt. % and mol. %., respectively. High purity powders of SiO_2 (purity >99.5%), $CaCO_3$ (>99.5%>), $MgCO_3$ (BDH Chemicals Ltd., UK, purity >99.0%), NH_6PO_4 (Sigma Aldrich, Germany, >99.0%) and CaF_2, MnO, CuO, and Y_2O_3 (Sigma Aldrich. Germany, 325 mesh. >99.9%), were used. Homogeneous mixtures of batches (~100 g) were obtained by ball milling, and then calcined at 900 ºC for 1 h. The calcined batch was melted in platinum (Pt) crucibles at 1580 ºC for 1 h in air. Glasses in bulk form were produced by pouring the melts into preheated bronze molds followed by annealing at 550 ºC for 1 h. The samples of the glass-powder compacts were produced from glass frits, which were obtained by quenching of glass melts in cold water. The frits were dried and then milled in a high-speed agate mill resulting in fine glass powders with mean particle sizes of ~20 μm (determined by light scattering technique; Coulter LS 230, Beckman Coulter, Fullerton CA; Fraunhofer optical model). Pellets with diameter of 10 mm and thickness of 2 mm were prepared by hand press.

Table 2.1 Batch compositions of all synthesized glasses in wt. %

Glass	CaO	MgO	P_2O_5	SiO_2	Y_2O_3	CaF_2	CuO	MnO	TiO_2
CaP-10	27.72	16.75	5.59	49.94				-	-
Y-1	27.44	16.58	5.53	49.44	1.00	-	-	-	-
Y-3	26.89	16.25	5.42	48.44	3.00	-	-	-	-
Y-5	26.33	15.91	5.31	47.45	5.00	-	-	-	-
F-1	27.44	16.58	5.53	49.44	-	1.00	-	-	-
F-3	26.89	16.25	5.42	48.44	-	3.00	-	-	-
F-5	26.33	15.91	5.31	47.45	-	5.00	-	-	-
Cu-1	27.44	16.58	5.53	49.44	-	-	1.00	-	-
Cu-3	26.89	16.25	5.42	48.44	-	-	3.00	-	-
Cu-5	26.33	15.91	5.31	47.45	-	-	5.00	-	-
Mn-1	27.44	16.58	5.53	49.44	-	-	-	1.00	-
Mn-3	26.89	16.25	5.42	48.44	-	-	-	3.00	-
Mn-5	26.33	15.91	5.31	47.45	-	-	-	5.00	-
Ti-1	27.44	16.58	5.53	49.44	-	-	-	-	1.00
Ti-3	26.89	16.25	5.42	48.44	-	-	-	-	3.00
Ti-5	26.33	15.91	5.31	47.45	-	-	-	-	5.00

Table 2.2 Batch compositions of all synthesized glasses in mol %

Glass	CaO	MgO	P_2O_5	SiO_2	Y_2O_3	CaF_2	CuO	MnO	TiO_2
CaP-10	27.76	23.34	2.21	46.68	-	-	-	-	-
Y-1	27.69	23.28	2.20	46.57	0.25	-	-	-	-
Y-3	27.55	23.16	2.19	46.33	0.76	-	-	-	-
Y-5	27.40	23.04	2.18	46.08	1.29	-	-	-	-
F-1	27.56	23.17	2.19	46.35	-	0.72	-	-	-
F-3	27.54	22.71	2.15	45.43	-	2.16	-	-	-
F-5	26.75	22.49	2.13	44.98	-	3.65	-	-	-
Cu-1	27.57	23.18	2.19	46.35	-	-	0.71	-	-
Cu-3	27.17	22.84	2.16	45.69	-	-	2.14	-	-
Cu-5	26.77	22.51	2.13	45.01	-	-	3.58	-	-
Mn-1	27.54	23.16	2.19	46.31	-	-	-	0.79	-
Mn-3	27.10	22.78	2.16	45.57	-	-	-	2.39	-
Mn-5	26.65	22.41	2.12	44.82	-	-	-	4.00	-
Ti-1	27.52	23.14	2.19	46.27	-	-	-	-	0.88
Ti-3	27.03	22.72	2.15	45.45	-	-	-	-	2.65
Ti-5	26.53	22.31	2.11	44.62	-	-	-	-	4.42

The amorphous/ crystalline nature of frits was confirmed by X-ray diffraction (XRD) analysis (Rigaku Geigerflex D/Max, Tokyo, Japan; C Series; CuK_a radiation; 2θ angle range 10º-50º; step 0.02º s^{-1}).

2.2 Structural characterization

2.2.1 Infrared spectroscopy

Infrared spectra of the glasses powder (before and after immersion in SBF) were obtained using an Infrared Fourier spectrometer (FT-IR, model Mattson Galaxy S-7000. USA). For this purpose glass powders were mixed with KBr in the proportion of 1/150 (by weight) and pressed into a pellet using a hand press. 64 scans for background and 64 scans per sample were made with signal gain 1. The resolution was 4 cm^{-1}.

2.2.2 Magic angle spinning (MAS)-Nuclear magnetic resonance (NMR) spectroscopy

The 29Si MAS NMR spectra were recorded on a Bruker ASX 400 spectrometer operating at 79.52 MHz (9.4 T) using a 7 mm probe at a spinning rate of 5 kHz. The pulse length was 2 μs and 60 s delay time was used. Kaolinite was used as the chemical shift reference. The 3IP MAS NMR spectra of glasses were recorded on a Bruker ASX 400

spectrometer operating at 161.97 MHz with 45º pulses, spinning rates of 12 kHz, a 60 s recycle delay and the chemical shift was quoted in ppm from phosphoric acid (85%).

2.3 In vitro bioactivity analysis

The in vitro bioactivity of the glasses, reflected in their capability of inducing HA formation onto their surfaces, was investigated by immersion of glass powders in simulated body fluid (SBF) (0.1 g glass powder in 50 ml SBF solution) at 37 ºC. SBF had an ionic concentration (Na^+ 142.0, K^+ 5.0, Ca^{2+} 2.5, Mg^{2+} 1.5, Cl^- 125.0, HPO_4^{2-} 1.0, HCO_3^- 27.0, SO_4^{2-} 0.5 mmol L^{-1}) nearly equivalent to human plasma, as discussed by Tas [47] and Kokubo et al. [48]. The powder-SBF mixtures were immediately sealed into sterilized plastic flasks and were placed in an oven at 37 ±0.5 ºC. The SBF solution was refreshed after every 48 h. The sampling took place after 1, 3, 6, 24 h, 3 and 7 days. The experiments were performed in triplicate in order to ensure the accuracy of results. After each experiment, the powders were separated from the liquids, washed by deionised water to stop the reaction, and then kept in the oven overnight to get dry powder. The apatite-forming ability of glass powders was followed by XRD and FTIR analysis.

2.4 Thermal characterization of the glasses

Dilatometry measurements were done with prismatic samples of the bulk glass with a cross-section of 4 x 5 mm^2 (Bahr Thermo Analyse DIL 801 L, Hiillhorst, Germany; heating rate 5 K min^{-1}).

Differential thermal analysis (DTA) of glass powders was carried out in air (DTA-TG, Labsys Setaram, Caluire, France) from room temperature to 1000 ºC at a heating rate (β) of 20 K min^{-1}) with α-alumina as reference material. The glass transition temperature (T_g), onset of crystallization (T_c), and peak temperature of crystallization (T_p) were obtained from DTA thermographs.

Circular pellets with 10 mm diameter, and 2 mm thickness were prepared by uniaxial pressing (80 MPa) of dry glass powders in a metallic mold. No binders or plasticizers were mixed with glass powders. The glass powder compacts were sintered for 1 h at 800, 850, and 900 ºC, respectively under non-isothermal conditions at a heating rate (β) of 5 K min^{-1}. The crystalline phase evolution in GCs was followed by powder diffraction XRD analysis (Rigaku Gei-gerflex D/Max, Tokyo, Japan; C Series; Cu kα, radiation; 2θ angle range 10º-50º; step 0.02º s^{-1}). Microstructure observations were done on polished (mirror finishing), chemically etched (by immersion in 2 vol. % HF solution for 2 min) surfaces of GCs by

field emission scanning electron microscopy (SEM; Hitachi SU-70, Tokyo, Japan) under secondary electron mode.

Archimedes' method (i.e., immersion in ethylene glycol) was employed to measure the apparent density of the bulk annealed glasses and sintered GCs. Molar volume (V_m) and excess volume (V_e) were calculated using the density data for the bulk glasses via following relations:

$$V_m = \frac{M}{\rho},$$

Where M is the molar mass of the glass and ρ is the apparent density of the bulk glasses. Similarly, excess volume of the glasses can be expressed as:

$$V_e = V_m - \sum_i x_i V_m(i)$$

Here, x_i is the molar concentration of every oxide, and $V_m(i)$ is the molar volume of every oxide (Table 2.3).

Table 2.3: Density and molar volume of glass components

Oxide	Density (gcm^{-3})	Molar weight ($g\ mol^{-1}$)	Molar volume ($cm^3\ mol^{-1}$)
MgO	3.6	40.3	11.19
CaO	3.34	56.07	16.79
SiO_2	2.65	60.07	22.67
MnO	5.37	70.94	13.21
CuO	6.31	79.55	12.61
TiO_2	4.23	79.87	18.88
P_2O_5	2.39	141.95	59.39
Y_2O_3	5.01	225.81	45.07
CaF_2	3.18	99.16	31.18

Chapter 3
Results and Discussion

3. Results and discussion

3.1 Glass forming ability

The melting of glass batches with all compositions mentioned in Table 2.1 at 1580 ºC for 1 h was adequate to obtain highly homogenous and transparent glasses for all the investigated compositions. The XRD analysis of the glasses confirmed their amorphous nature except for sample Ti-5 which showed some traces of crystallinity as has been shown in Fig. 3.1 The idea behind choosing 5 wt. % to be analysed by XRD of all doped glasses is to confirm the glass forming ability with the higher added amount of the doping oxides and ensure crystalline free glasses for higher doping wt. % which differ from the parent glass composition.

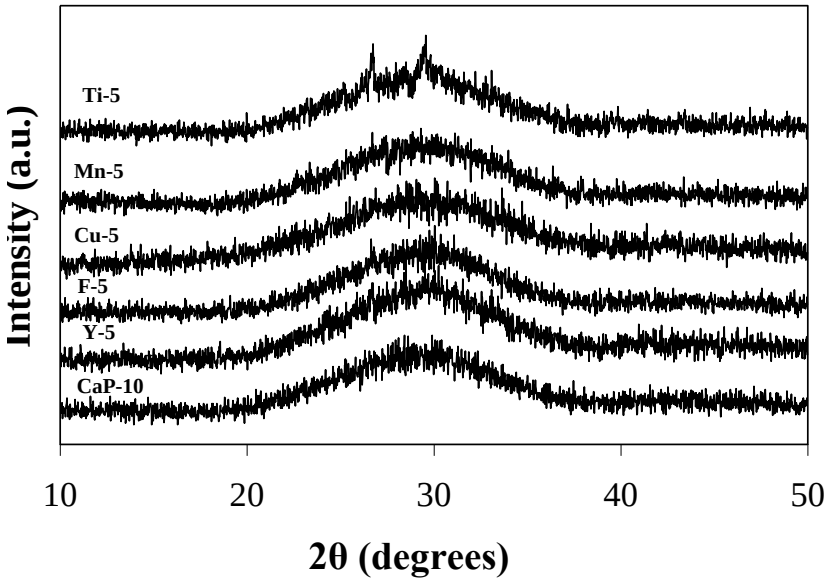

Fig. 3.1 X- ray diffractogram confirms amorphous phase for doped glasses.

3.2 Density of glasses

The incorporation of additives to the parent glass CaP-10 increased the glass density (ρ) irrespective of the nature of additive as is evident from Table 3.1 In the investigated glasses, Cu, Mn and Y-containing glasses exhibited higher densities in comparison to their F and Ti-containing counterparts. The density is an additive property and increases with incorporation of additive with higher density. The values for molar volume (V_m) and excess volume (V_e) of all the glasses are presented in Table 3.1

Table 3.1 Density, molar volume, and excess volume for the investigated glasses

Sample	Density	Mol vol.	Excess vol.
CaP-10	2.86±0.01	19.64±0.04	-0.08±0.04
F-1	2.86±0.01	19.62±0.09	-0.14±0.09
F-3	2.88±0.01	19.66±0.02	-0.17±0.02
F-5	2.90±0.01	19.66±0.01	-0.24±0.01
Y-1	2.88±0.003	19.68±0.02	-0.11±0.02
Y-5	2.94±0.01	19.85±0.04	-0.2±0.04
Cu-1	2.87±0.01	19.59±0.03	-0.08±0.03
Cu-3	2.92±0.01	19.43±0.03	-0.14±0.03
Cu-5	2.93±0.01	19.42±0.04	-0.05±0.04
Mn-1	2.88±0.001	19.56±0.01	-0.12±0.01
Mn-3	2.91±0.003	19.43±0.02	-0.14±0.02
Mn-5	2.95±0.001	19.26±0.01	-0.2±0.0.01
Ti-1	2.88±0.01	19.59±0.05	-0.13±0.05
Ti-3	2.89±0.01	19.60±0.04	-0.11±0.04
Ti-5	2.91±0.004	19.61±0.03	-0.09±0.03

The incorporation of almost all the additives in glasses led to a gradual decrease in their excess volume while their molar volumes either remained constant or decreased, respectively. The excess volume is determined mainly by the distribution in bond lengths, angles, and coordination numbers in the short range structure [49]. The decrease in excess volume with increasing the amount of additives suggests that the average bond length is becoming shorter. Also the incorporation of additives might lead to phase separation. As an example of this phenomenon, the additions of titanium oxide to base glass have been reported to lead to phase separation [50], while other authors [51] reported that TiO_2 can also improve glass-forming ability, chemical durability and stabilization of glass structure. These observations are somewhat contradictory and might result from the specificities of the compositions used. As a matter of fact, titania has been often used as nucleating agent in glass compositions [52].

3.3 Structure of glasses

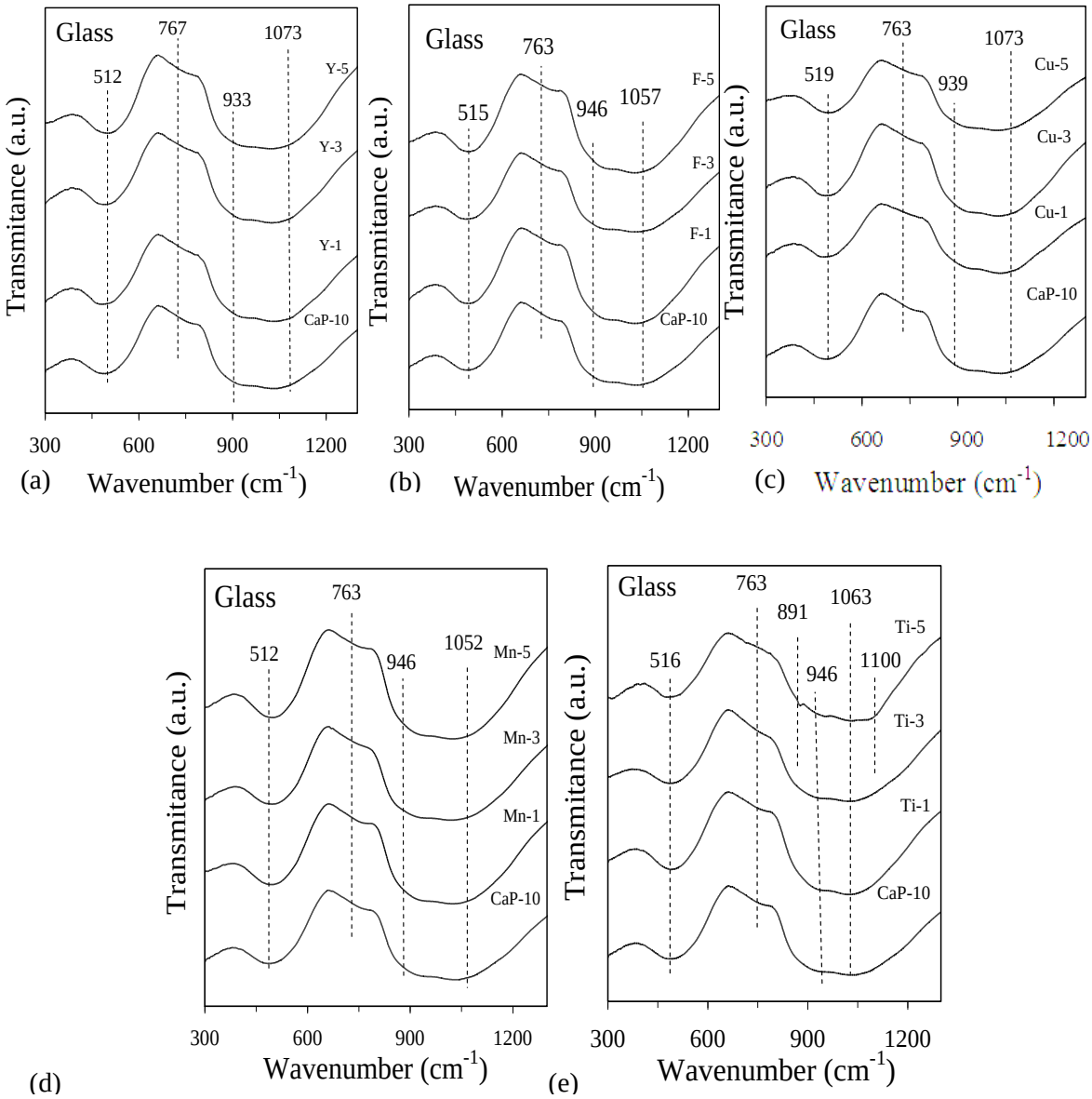

Fig. 3.2 FTIR spectra of all the glasses before immersion in SBF.

It has been well established that molecular structure of glasses plays a crucial role in deciding their bioactivity. For example: the bioactivity of 45S5 Bioglass® is known to arise from a structure dominated by chains of Q^2 metasilicates, which are occasionally cross-linked through Q^3 units, whereas Q^1 species terminate the chains [14], where Q^n

species distribution furnishes a measure of the connectivity of the glass network and the index *n* refers to the number of bridging oxygens (BOs) surrounding a network former ions. Similarly, the enhanced dissolution of silica in highly bioactive compositions has also been found to be closely related to the significant fraction of Q^1 (Si) chain terminators while moderate bioactivity can be achieved when Q^3 (Si) structures predominate [14]. Therefore, understanding these features allows designing new glasses with improved chemical durability and tailored biodegradability for specific applications.

The room-temperature FTIR spectra of all the investigated glasses are presented in Fig. 3.2. In general, all the FTIR spectra of all the glasses exhibit three broad transmittance bands in the region 300-1300 cm^{-1}. The most intense bands lie in the 800-1300 cm^{-1} region, the next one between 300 and 600 cm^{-1}, while the least intensive lies between 650 and 800 cm^{-1}. This lack of sharp features is indicative of the general disorder in the silicate and phosphate network mainly due to a wide distribution of Q^n units occurring in these glasses. The most intense bands in the 800-1300 cm^{-1} region correspond to the stretching vibrations of the SiO_4 tetrahedron with a different number of bridging oxygen atoms [53]. It should be noted that the band near ~1050 -1070 cm^{-1} may also be attributed to PO_3 end groups due to the presence of P_2O_5 glass network former in the investigated glasses. Further, the ~500 cm^{-1} band can be attributed to Si-O-Si bending modes [54], while the weak ~760 cm^{-1} shoulder may be due to Si–O–Si symmetric stretching with simultaneous Si cation motions [55].

Since the chemical composition of glass CaP-10 is very close to diopside, we can expect almost similar structural organization in this glass too. Further, the ^{31}P MAS-NMR spectra of all the glasses show a predominance of an orthophosphate-type environment. This minimizes the possibility of re-polymerization in the silicate glass network in the form of Si-O-Si or Si-O-P linkages due to the presence of phosphate component as suggested experimentally by Lockyer et al. [56] and computationally by Tilocca [14]. Also, these results are in good co-relation with those reported by Lusvardi et al. [18] and Linati et al. [17] for the 45S5 glass where it has been deduced a fraction of orthophosphate units of ~82% while the rest might be comprised of meta- or pyrophosphates.

Fig. 3.3 shows the ^{29}Si and ^{31}P MAS-NMR spectra of the parent glass CaP-10. The ^{29}Si spectrum for the parent glass (Fig. 3.3a) depict the dominance of Q^2 (Si) structural units in the glasses [57].

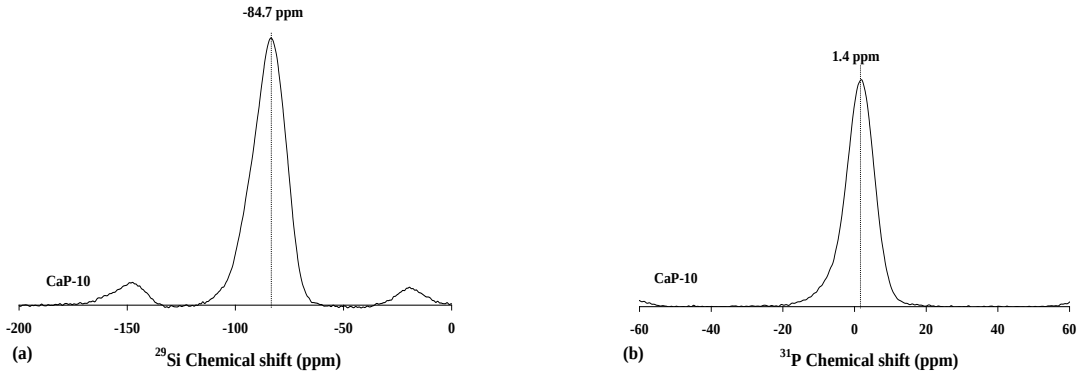

Fig. 3.3 (a) 29Si and (b) 31P MAS-NMR spectra of CaP-10 glass

In particular, the broad ^{29}Si spectra for the parent glass implying towards a wider distribution Q^n (Si) species in the glass structure. The ^{31}P MAS-NMR spectra's of parent glass shows a predominance of an orthophosphate-type environment (Fig. 3.3b). In fact, the observed chemical shifts, 1–3 ppm, are close to that of the calcium orthophosphate (3.1 ppm) and that of the amorphous magnesium orthophosphate (*ca.* 0.5 ppm) [53].

No significant differences in the ^{29}Si and ^{31}P NMR spectra of all glasses were observed after doping the parent glass with different additives (Fig. 3.4, Fig. 3.5, Fig. 3.6, Fig. 3.7 and Fig. 3.8) except that the peak of ^{29}Si spectra in almost all the glasses shifted to -83.7 ppm from -84.7 ppm, thus depicting a slight depolymerisation in the glass network.

The following observations were recorded with respect to the influence of additives on the structural behaviour of investigated glasses:

i) In the case of Yttrium doped glasses, although we could not observe any significant differences in the molecular structure of glasses possibly due to very low content of Y_2O_3 (0.25 – 1.29 mol.%), the change in chemical shift (~1 ppm) of ^{29}Si NMR spectra fig. 3.4(a) with yttrium incorporation reveals the depolymerising effect of Y^{3+} on the glass structure. Christie et al. [30] has been demonstrated that Y^{3+} ion prefers to coordinate in pseudo-octahedral coordination at the expense of other modifier cations due to its higher field strength 0.6 versus 0.53 for Mg^{2+} (4-fold

coordination) or 0.46 versus 0.33 for Ca^{2+} (6-fold coordination). A related effect has previously been found to control the coordination and site selectivity of calcium and sodium in Y-free silicate glasses, with important consequences for the mechanism of cations migration [30].

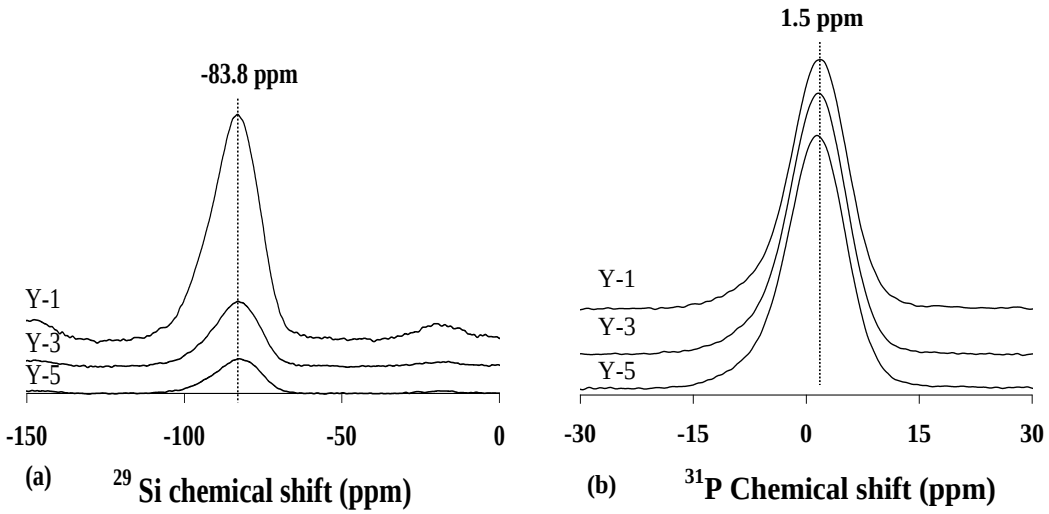

Fig. 3.4 (a) ^{29}Si and (b) ^{31}P MAS-NMR spectra of Y (1-3-5) glass series

ii) In the case of fluoride doped glasses, it is noteworthy that the possibility of the formation of Si-O-P bonds is low if not negligible (as depicted by almost negligible shift in the ^{29}Si spectra). In fact, according to the NMR results, phosphate groups are not part of the actual glass network backbone. Similar results have also been obtained by Brauer et al. [57] on a series of SiO_2-P_2O_5-CaO-Na_2O-CaF_2 glasses where it was found that addition of CaF_2 did not disrupt the network connectivity by forming Si-F bonds, instead, formed mixed calcium sodium fluoride species. However, it should be noted that bioactivity is not solely a function of glass structure, but also depends on their chemical nature [58].

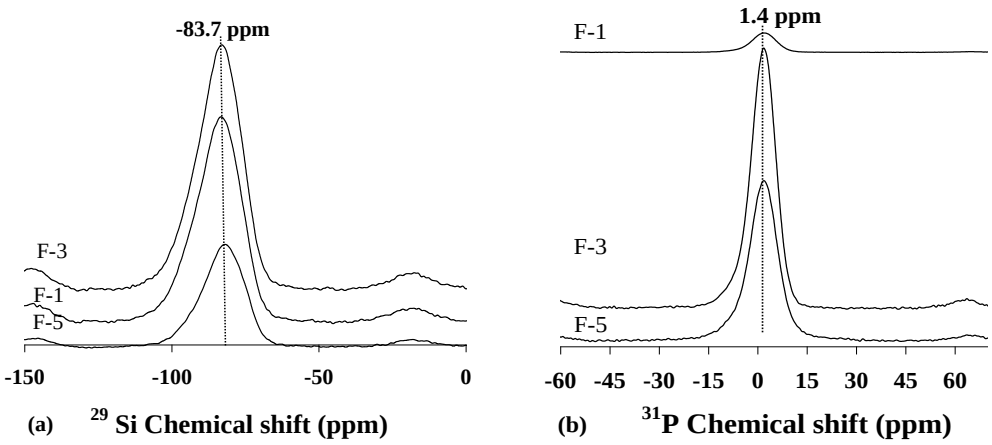

Fig. 3.5 (a) ^{29}Si and (b) ^{31}P MAS-NMR spectra of F (1, 3, 5) glass series

iii) The structure of glasses plays a crucial role in deciding their ion release behaviour; especially the release of copper ion from glass in aqueous medium is controlled by its coordination environment and its clustering behaviour.

In the present study, although we could not observe any significant differences in the molecular structure of glasses possibly due to very low content of CuO (0.71 – 3.58 mol.%), where the change in chemical shift (~1 ppm) of ^{29}Si NMR spectra with copper incorporation reveals the depolymerising effect of Cu^{2+} on the glass structure, the ^{31}P NMR spectra indicate that a portion of CuO, which acts mostly as a network modifier [59], enters the glass network to form covalent P-O-Cu linkages in the polyphosphate glasses.

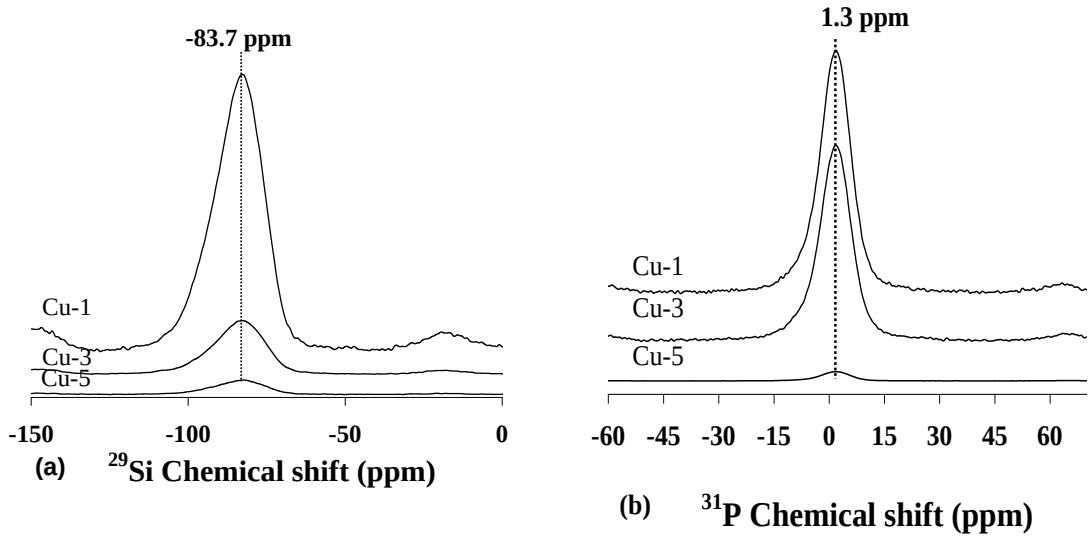

Fig. 3.6 (a) ^{29}Si and (b) ^{31}P MAS-NMR spectra of Cu (1, 3, 5) glass series

iv) Also it has been reported that the introduction of manganese in the phospho-silicate glass network is known to induce significant changes in the local oxygen environment since the donor ability of manganese is weaker in comparison to oxide, making the possibility of Si-Mn formation, unlikely. The molar percentages of MnO that have been added to the parent glass are very small (0.79-4) mol %, while the structure of the parent glass dominated by Q^2, is shifted from Q^2 to Q^1 or shared in-between with high Q^2 % approaching 75% by increasing MnO content in the composition, as determined by Raman spectroscopy [60].

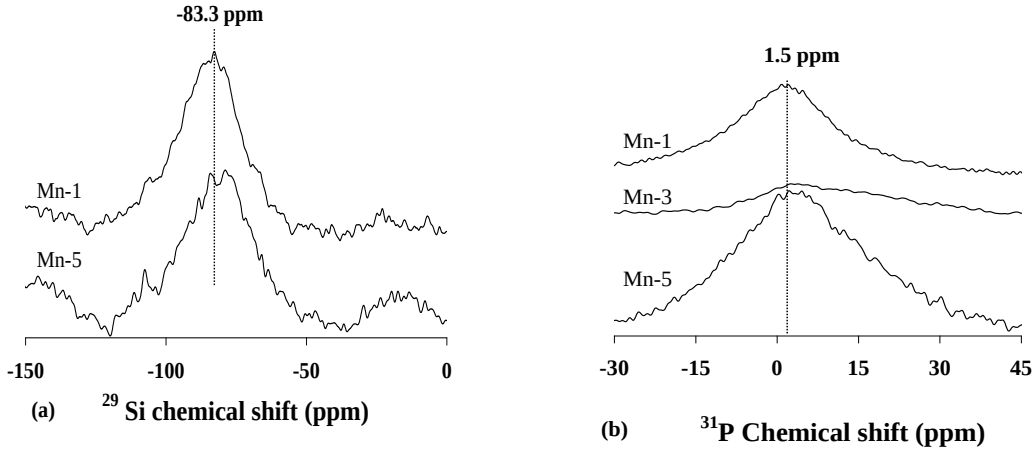

Fig. 3.7 (a) ^{29}Si and (b) ^{31}P MAS-NMR spectra of Mn (1, 3, 5) glass series

v) In the case study of titanium doping glasses, although we could not observe any significant differences in the molecular structure of glasses possibly due to very low content of TiO_2 (0.88 – 4.42 mol.%), the change in chemical shift (~1 ppm) of ^{29}Si NMR spectra with titanium incorporation reveals the depolymerising effect of Ti^{3+} on the glass structure. In alkali/Alkali earth silicate glasses, it has been reported that Ti was found in 4-6 folds coordination in glass structure as mentioned by (Wood and Hess) [61]; (Furukawa and White, 1979); and Mysen et al, [62]. Characterization of the Ti-glass phase has also revealed that the addition of TiO_2 results in an increased concentration of Si- NBO species [63].

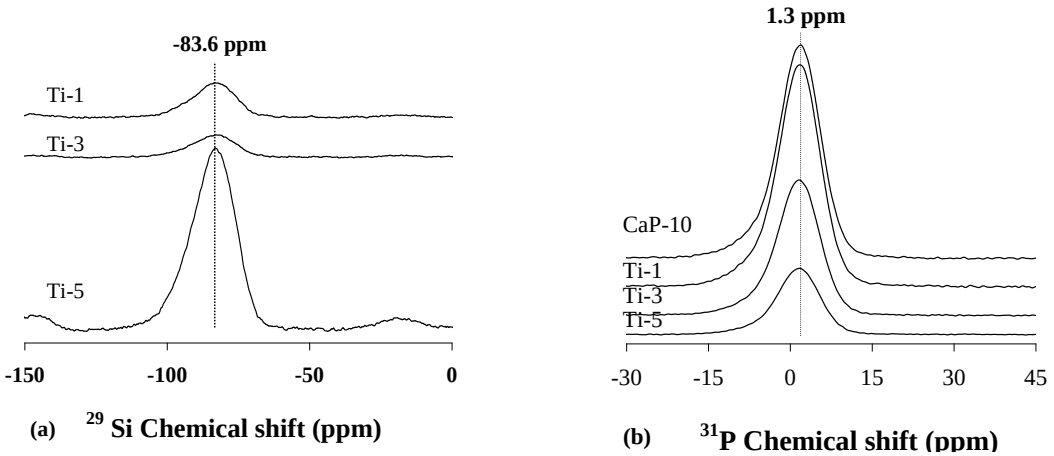

Fig. 3.8 (a) ^{29}Si and (b) ^{31}P MAS-NMR spectra of Ti (1, 3, 5) glass series

In the present study, all the glasses exhibit the dominance of Q^2 (Si) species in the silicate glass network thus implying towards high rate of bioactivity (usually marked by apatite forming ability on glass surface). It has been reported that in an amorphous diopside glass, the distribution of Q^n (Si) is: 28% Q^1, 43% Q^2, 25% Q^3 and 4% Q^4 [40]. This distribution of Q^n (Si) species in diopside glass is quite close to the Q^n (Si) distribution of the 45S5 glass (15% Q^1, 67% Q^2, 18% Q^3) calculated by Linati et al. [17] since a mixture of (Q^1 + Q^2) units predominate in both cases, thus giving an indication of good bioactivity.

3.4 Thermal behaviour of glasses

3.4.1 Dilatometry

The CTE values of glasses as obtained from dilatometry in the temperature interval of 200 – 500 ºC varied between about (7.8-10.5) x 10^{-6} K^{-1}). (Fig. 3.9) The CTE values of almost all the glasses (except Mn containing glasses) depicted a decrease with initial addition of additives (1 wt. %) before exhibiting an increase with further additions. However, an opposite trend was observed for Mn containing glasses which exhibited an increase in CTE values with the initial 1 wt. % addition, while further additions of MnO in glasses led to a gradual decrease in CTE values.

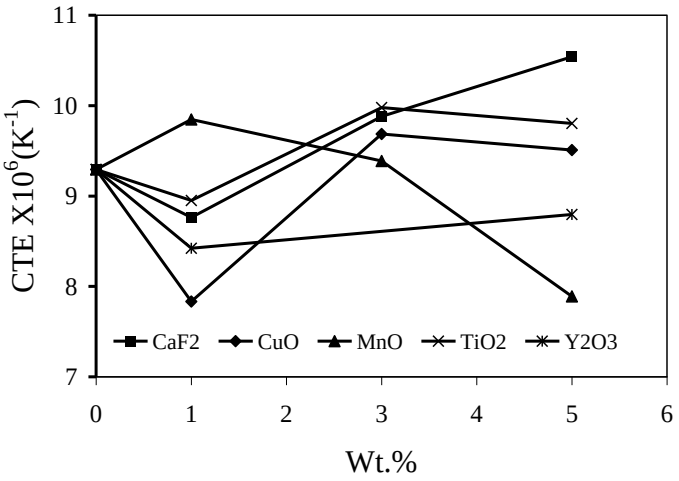

Fig. 3.9 Dilatometry results for the investigated glasses

3.4.2 Differential thermal analysis (DTA)

Bioactive glasses are not single-phase systems having one glass transition temperature. Instead, they have undergone amorphous phase separation, or glass-in-glass phase separation, to give a two-phase system consisting of a silicate glass matrix phase in which an orthophosphate droplet glass phase is dispersed [64].

The glass transition temperature (T_g) is an important parameter for characterizing bioactive glasses, as it is an indirect measure of the connectivity of the glass network and therefore is closely related to glass solubility and degradation, crystallization and mechanical properties [64].

Fig. 3.10 presents a typical DTA thermograph for the parent glass CaP-10 at a heating rate (β) of 20 K min^{-1}. An endothermic dip in the temperature interval of 725 – 785 ^oC corresponding to glass transition (T_g) can be seen before the onset of crystallization (T_c) followed by a well-defined single exothermic crystallization peak. The presence of the single crystallization exotherm anticipates that the glass-ceramic is formed either as a result of single phase crystallization or of an almost simultaneous precipitation of different crystalline phases. Similar behaviour was observed in all the investigated glasses as is evident from Fig. 3.11. The incorporation of additives led to a decrease, an increase, or no effect in T_g Values.

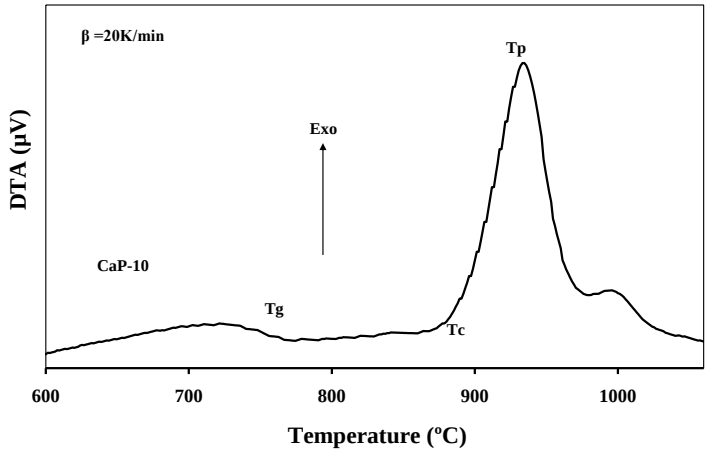

Fig. 3.10 DTA thermograph for CaP-10 at heating rate (β) of 20 K min^{-1}

The following observations were recorded with respect to the influence of additives on the thermal behaviour of investigated glasses:

i) All Y_2O_3 containing glasses exhibit T_g values that are lower than the parent glass composition, CaP-10. However, the increasing weight percentages of Y_2O_3 in the glasses result in slight increases on the value of glass transition temperature (T_g) (as obtained from the mid-point of endothermic dip before onset of crystallization in DTA thermograph) as it varies in the range 769-775 °C for this glass series. A gradual increase in the T_p values could be observed with increasing Y_2O_3 content in the glasses up to Y-3, therefore gradually enhancing the stability of the glasses against devitrification, while a further Y_2O_3 addition to 5 wt. % reversed this trend. The increase in T_g with addition of Yttrium to glasses can be explained by the high fraction of Si-O-P linkages as has been deduced from the structural studies on these glasses. The trend of T_g can be explained by taking into account that, according to Ray [65], the glass transformation temperature depends on the density of covalent cross-linking and the number and strength of the cross-links between the cation and oxygen atoms. The increase in T_g can therefore be ascribed to the greater strength of the cross-links between the Y^{3+} cation and oxygen atoms [66].

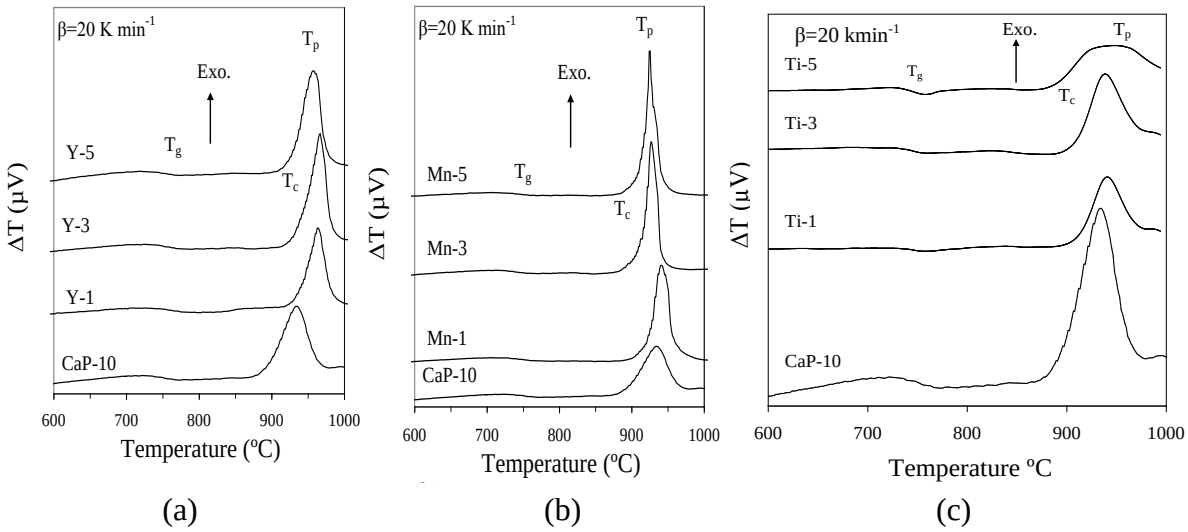

Fig. 3.11 DTA thermographs of the investigated at β = 20 K min^{-1}, (a) Y- containing glasses; (b) Mn-containing glasses; and (c) for Ti-containing glasses.

ii) The addition of CaF_2, CuO, MnO and the increase of their weight percentage in the glasses caused decreases on the values of glass transition temperature (T_g) (as obtained from the mid-point of endothermic dip before onset of crystallization in DTA thermograph) as it varies in the range 738-766 ºC for this three series of glasses. However, the T_g values of all these doped glasses were evidently lower than their parent glass composition, CaP-10. In a similar way, the same additions also resulted in decreases of the onset of crystallization temperature (T_c) that varied in the range of (842-889 ºC). A gradual decrease in the T_p values could be also observed with increasing doping weight percentages in the glasses. For the CaF_2 containing glasses, the decrease in T_g with increasing wt. % of CaF_2 to parent glass can be explained by the low fraction of Si-O-P linkages as has been deduced from the structural studies on these glasses. Further, in fluoride free glass, divalent modifier ions bind together silicate anions by electrostatic forces and the modifier ions effectively act as ionic bridges between two NBOs. However, with addition of CaF_2 in glasses, the fluorine is complexing with calcium or magnesium, thus, hypothetical CaF^+ and MgF^+ species are added to the silicate ions which reduce the electrostatic forces between NBOs considerably and results in a decrease in T_g [57], the degree of polymerisation is expected to decrease and, accordingly, T_g values should decrease and increasing CTE of glasses. By the same manner the increase in

weight percentage for both CuO, and MnO doped glasses tend to decrease the (T_g) gradually, and degree of polymerization is expected to be decreased consequently, sharing the same trend for the these three types of doped glasses.

iii) The variation in titanium concentration in glasses caused no change on value of glass transition temperature (T_g) (as obtained from the mid-point of endothermic dip before onset of crystallization in DTA thermograph) for the studied glasses. A decrease in intensity of the exothermic peak and a shift of T_p values to higher temperatures could be observed with adding 1 wt. % of TiO_2 to the parent glass (Ti-1). This means that the thermal stability parameter ΔT (= $T_c - T_g$) was enhanced for this first addition thus, providing wider processing window for a glass composition to attain maximum densification upon sintering. But this situation was somewhat reversed by adding further amounts of TiO_2. The differences are still small for the Ti-3, but became exacerbated for the composition Ti-5. As a matter of fact, T_c significantly decreased while the resulting crystallization exotherm is no more a relatively sharp peak but a broad band. This means a degradation of the sintering ability and that the glasses containing the higher amounts of TiO_2 are more prone to crystallization. In other words, TiO_2 is playing a nucleating agent role, often referred to in literature reports [52]. These variations in DTA thermographs and their implications in the sintering/crystallization behaviour are consistent with a decreased diffusivity of the larger ionic radius Ti^{+4} in octahedral coordination (0.61 Å) [67]. Physical properties of the parent glass show some evidence for a change in the structural role of titanium with increasing titanium content. Glass transition temperature T_g doesn't exhibit any change by increasing the titanium content in the parent glass. Our results for T_g are consistent with the work reported elsewhere [50, 51]. This non change of T_g suggests that viscosity should be about the same in all cases.

Table 3.2 T_g, T_c, and T_p values for all investigated glasses

Glass	Tg	Tc	Tp	$\Delta = T_c - T_g$
CaP-10	776	869	934	93
Y-1	769	898	958	129
Y-3	773	910	966	137
Y-5	775	915	964	140
F-1	765	874	941	109
F-3	745	870	941	125
F-5	738	862	921	124
Cu-1	765	881	950	116
Cu-3	753	854	924	101
Cu-5	746	842	904	96
Mn-1	766	889	942	123
Mn-3	764	875	926	111
Mn-5	762	868	925	106
Ti-1	760	893	942	133
Ti-3	760	889	940	129
Ti-5	760	875	950	115

3.5 In vitro bioactivity in SBF

In relation to bioactivity, network modifying alkali and alkali earth cations in the glass can disrupt the continuity of the glass network due to the breaking of some of the Si-O-Si groups leading to the formation of Si-NBO species [63]. The presence of these Si-NBO groups favours the ion exchange process where dissolution of the soluble silica content results in the formation of a SiO_2 rich surface layer and consequently Si-OH groups, and also the release of cations from the glass surface [63].

The immersion of glass powders in SBF solution for 1 h led to the formation of hydroxyapatite (HA; $Ca_5(PO_4)_3(OH)$; ICDD: 09-0432) on their surface in Y_2O_3, MnO, CuO and TiO_2 containing glasses, respectively, while silica (S; SiO_2; ICDD: 073-3462) has been formed on the surface of (Mn-5), while Calcite (C; $CaCO_3$;ICDD: 00-005-0586) and Calcium Phosphate (CaP, $Ca_2P_2O_7$,ICDD:00-009-0346) have been formed on the surface of (Y-5) as depicted by XRD data in Fig. 3.12. Also, the FT-IR spectra of all the investigated glasses showed considerable differences in comparison to Spectra of their respective parent glasses (Fig. 3.2), after soaking in SBF solution for 1 h (Fig. 3.13).

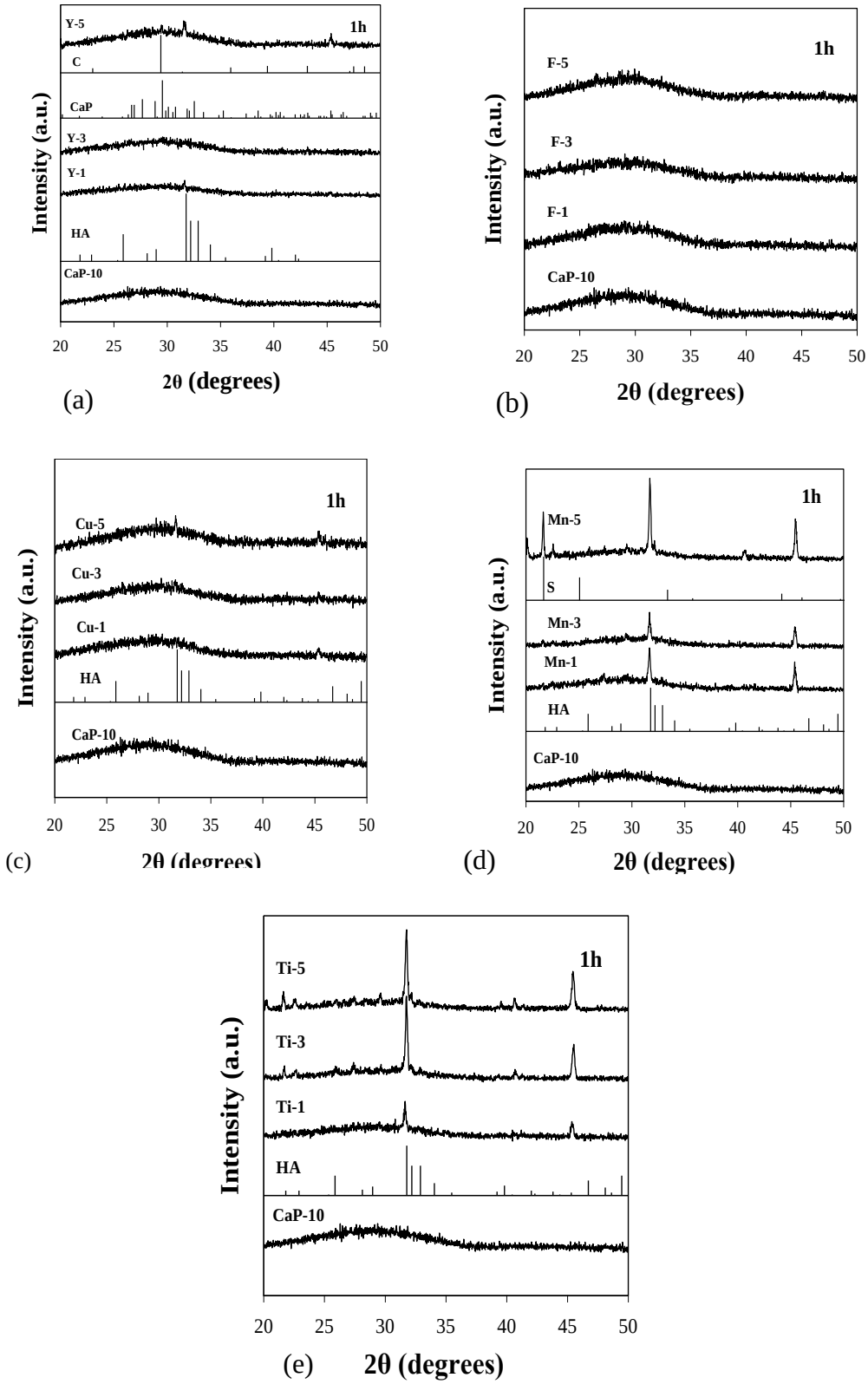

Fig. 3.12 X- ray diffractogram of all investigated glasses after immersion in SBF for 1 h

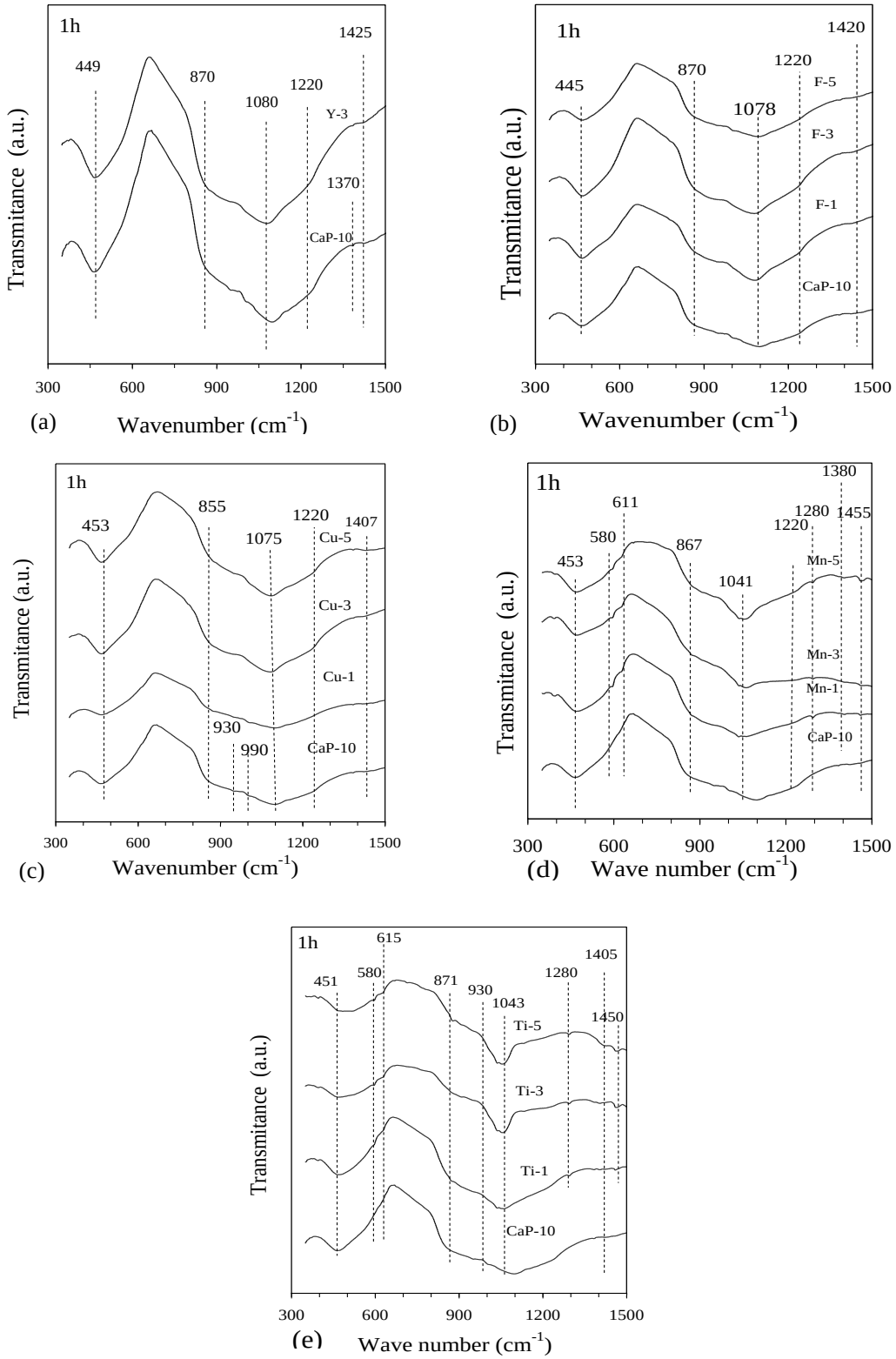

Fig. 3.13 FTIR for all glass powders after 1h of immersion in SBF.

As is evident from Fig. 3.13, a strong low frequency band centred at ~ 450 cm^{-1}, ascribed to a deformation mode of silica layer that develops on the dissolving glass particles could be seen in all the glasses after immersion in SBF solution for 1 h [12]. The main IR band now occurs at 1080 cm^{-1} and a nearby shoulder, centred at ~1220 cm^{-1} and attributed to Si-O-Si vibration [68], can be observed in all the glasses, due to the interfacial formation of high-area silica gel layer, as postulated in Hench's inorganic reaction set [69]. Further, two small peaks could be observed in Mn and Ti-containing glasses at ~580 cm^{-1} and 615 cm^{-1}. This is the most characteristic region for apatite and other phosphates as it corresponds to P-O bending vibrations in a PO_4^{3-} tetrahedron. Apatitic PO_4^{3-} groups have characteristic split bands at ~560 and 600 cm^{-1}, with a third signal at ~575 cm^{-1} observed for crystallites of small size [70]. Furthermore, a band at in the range 1400-1450 cm^{-1} along with another one at ~850-870 cm^{-1} present in all glasses might correspond to formation of complex carbonate species connected with the presence of Ca^{2+} ions in the surface [13], or to the incorporation of carbonate into the phosphosilicate layer [70]. It should be noted that broad CO_3^{2-} band at ~ 1440 cm^{-1} observed in most of the investigated glasses after immersion in SBF indicate towards A-type substitution (i.e. carbonate replacing a hydroxyl group). The CO_3^{2-} signal for B-type substitution (i.e. carbonate replacing phosphate group) would be shifted to lower wave numbers, starting from ~ 1410 cm^{-1} [12]. An increase in immersion time (1 h – 7 days) led to the gradual precipitation and dissolution of HA and calcite on the glass surface as depicted by XRD analysis (Table 3.3). Interestingly, fluoride containing glasses showed the slowest rate of HA formation among all the investigated glasses. The yttrium containing glass exhibited high rate of apatite formation as is evident from Fig. 3.12 and Table 3.3. The FT-IR data reveals the formation of silica gel layer on glass surface after 1 h of immersion in SBF solution while all the glasses exhibited HA formation between 1-3 h of their immersion in SBF solution. With prolonged immersion of glass in SBF solution for 6 and 24 h, the HA dissolution took place while it re-precipitated after 3 days and continued to exist until 7 days of immersion in SBF solution (Table 3.3). Since, intense ionic exchanges occur at the bioactive glass surface that cause major changes in the degree of super-saturation for HA formation in biological fluids; therefore, the potential for each glass to form an apatite layer can be extrapolated from the corresponding evolution of super-saturation degree. According to Lao et al. [71], super-

saturation degree may be defined as: SD = Q/K_{sp}, where K_{sp} is the solubility product of HA in aqueous solution while Q is the ionic activity product for the formation of HA.

Therefore, the solution and HA mineral phase reach equilibrium when SD = 1. For SD < 1, the dissolution of HA mineral phase is favoured; while the solution is supersaturated with respect to HA mineral and its precipitation is favoured when SD > 1. In the present scenario, during initial hours of immersion of glass in SBF, the SD increases because of dealkalinazation of glass surface while formation of silica rich layer provides regions of low interfacial energy, thus providing favourable sites for nucleation of HA. However, disappearance of HA after 6 h of immersion in SBF solution may be attributed to the changing degree of super-saturation owing to the refreshing of SBF solution after every 48 h.

Table 3.3 Crystalline phases evolution on the glass surface after immersion of glasses in SBF solution for various time durations. (HA: Hydroxyapatite; C: Calcite; S: silicate; Cap: Calcium Phosphate; A: Amorphous).

	1h	3h	6h	24h	72h	168h
CaP-10	A	C; HA	A	A	HA	HA
Y-1	C; HA	C; HA	A	A	HA	HA
Y-3	A	C; HA	A	A	A	HA
Y-5	C; CaP; HA	C; HA	A	A	HA	HA
Cu-1	A	C; HA	A	A	A	HA
Cu-3	A	HA	A	A	HA	HA
Cu-5	HA	C; HA	A	A	HA	HA
F-1	A	A	A	A	A	HA
F-3	A	A	A	A	A	A
F-5	A	HA	A	A	A	HA
Mn-1	HA	HA	A	A	A	A
Mn-3	HA	A	A	A	A	A
Mn-5	HA; S	HA	A	A	A	A
Ti-1	HA	HA	A	A	A	A
Ti-3	HA	HA	A	A	A	A
Ti-5	HA	HA	A	A	A	A

A contradictory behaviour has been reported by Cacaina et al. [72] where it has been shown that increasing Y_2O_3 content in glasses decreases their apatite forming ability in SBF solution. However, the difference in results may be attributed to the significantly higher Y_2O_3 content used by Cacaina et al. [72] in their glasses (~9-15 wt.%) which should lead to clustering of Y^{3+} ions, thus resulting in stabilizing the structure and retarding the dissolution of glasses.

The introduction of fluoride in the phospho-silicate glass network is known to induce significant changes in the local oxygen environment since the donor ability of fluoride is weaker in comparison to oxide, making the possibility of Si-F formation, unlikely. Therefore, under such conditions, fluoride remains predominantly in ionic state and prefers to form ionic bonds with metal cations (Ca and Mg in present study), thus avoiding the de-polymerization of silicate glass network and forcing phosphate groups to link with silicate groups, leading to higher glass connectivity [18] which might further hamper their bioactivity.

With regard to slow apatite forming ability of fluoride containing glasses, similar behaviour has been observed by Kansal et al. [6] as well as by Lusvardi et al. [13]. This behaviour may be explained on the basis of decreasing tendency towards formation of silica gel like layer (considered to be essential in order to activate the apatite nucleation) on the glass surface with increasing fluoride content as is evident from Fig. 3.13b. Similar results were also reported on $CaO\text{-}SiO_2$ based glasses by Ebisawa et al. [73] where it was shown that fluoride addition to these glasses lowered their apatite forming ability and silica gel layer formation was either small or not observed. Therefore, lack of HA formation in the present study does not render the fluoride containing glasses to be bio-inert. Instead, detailed investigations need to be carried out in vitro and in vivo in order to determine the precise influence of fluoride on bone regeneration.

Ti-based materials are also known to form a CaP surface layer when immersed in simulated body fluids [74]. The presence of this layer is reported to be a prerequisite to bone bonding [75]. Ti-based glass exhibited high rate of apatite formation as is evident from Fig. 3.12 and Table 3.3. The FT-IR data reveals the formation of silica gel layer on glass surface after 1 h of immersion in SBF solution while all the glasses exhibited HA formation between 1-3 h of their immersion in SBF solution. With prolonged immersion of glass in SBF solution for 6 and 24 h, also for 3 and 7 days the HA dissolution took place as has been shown in (Table 3.3). Since, intense ionic exchanges occur at the bioactive glass surface that cause major changes in the degree of supersaturation for HA formation in biological fluids; therefore, the potential for each glass to form an apatite layer can be extrapolated from the corresponding evolution of supersaturation degree as demonstrated by Lao et al. Also it has been clear enough from x-ray that increasing TiO_2 content in glasses increases their apatite forming ability in SBF solution.

3.6 Sintering and crystallization behaviour of glasses

In agreement with the ΔT (= $T_c - T_g$) values as obtained from DTA data (Table 3.2), well sintered, dense but amorphous glass powder compacts were obtained after sintering at 800 ºC for 1 h as is evident from the XRD data presented in (Fig. 3.14 (a, b, d, e) while (c) has crystalline phase of (Di; $CaMgSi_2O_6$; ICDD: 78-1390).

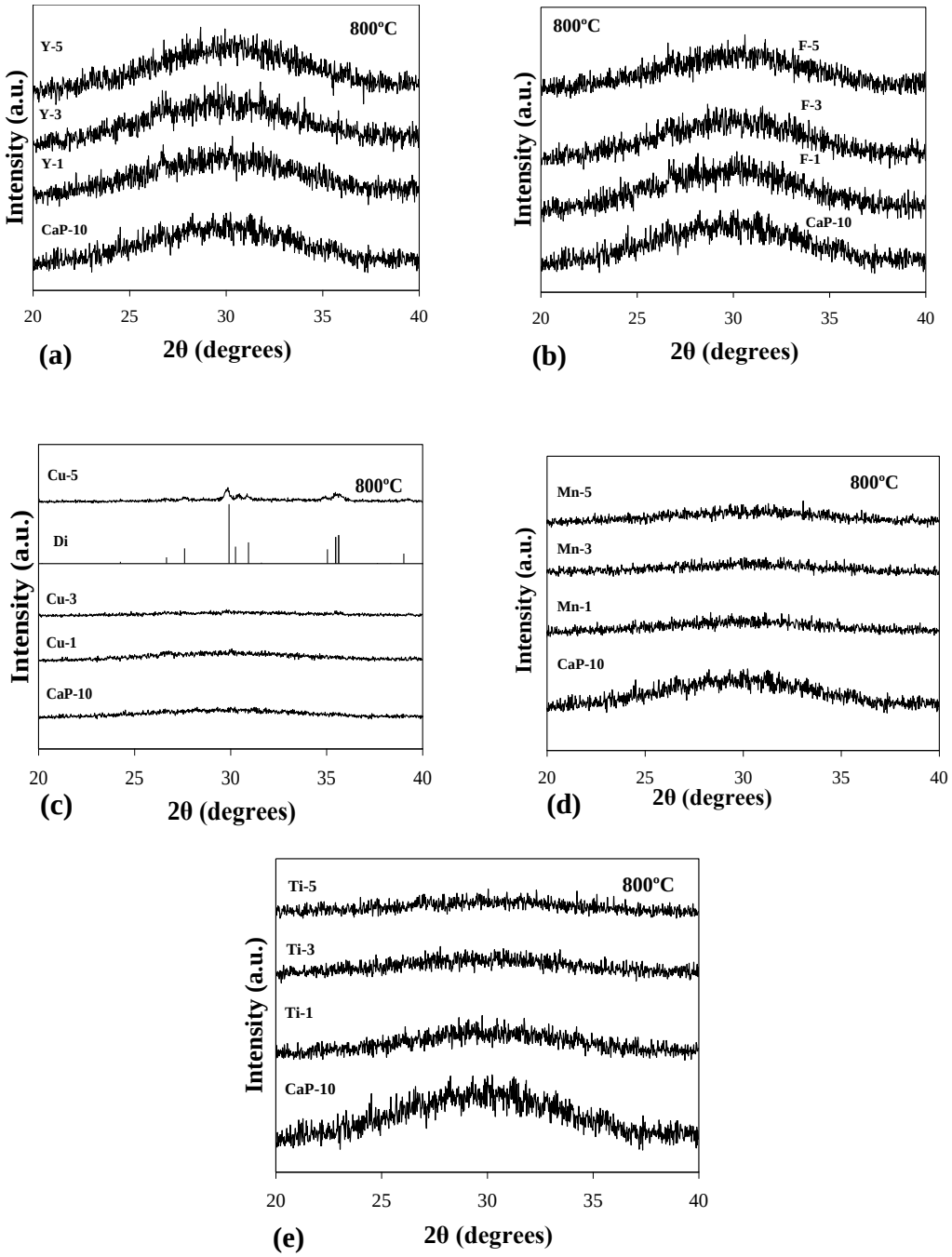

Fig. 3.14 X- ray diffractogram of glass powder compacts after sintering at 800ºC for 1 h

Further increase in temperature to 850 ºC (Fig. 3.15) led to the crystallization of diopside (Di; $CaMgSi_2O_6$; ICDD: 78-1390) as the primary crystalline phase in all the glass-ceramics.

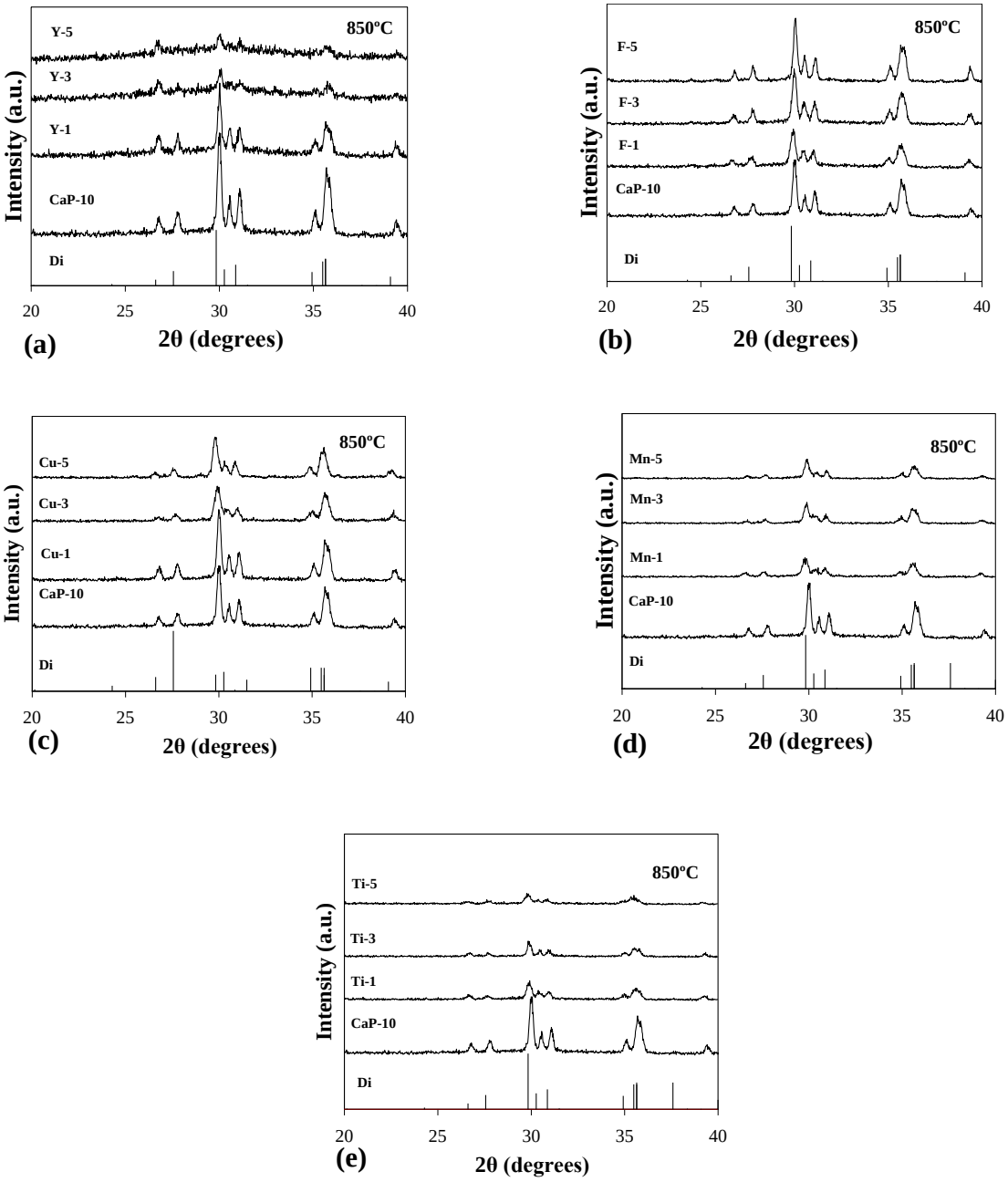

Fig. 3.15 X- ray diffractogram of glass powder compacts after sintering at 850ºC for 1h

With further increase in temperature i.e. 900 ºC the intensity is increased of the Di crystalline phase, and evolution of Yttrium oxide (YO; Y2O3; ICDD: 044-0399) and Fluorapatite (FA; $Ca_5(PO_4)_3F$; ICDD: 01-073-1727) crystalline phases in yttrium and Fluoride glasses respectively, (Fig. 3.16) indicating the possible increase in crystallinity.

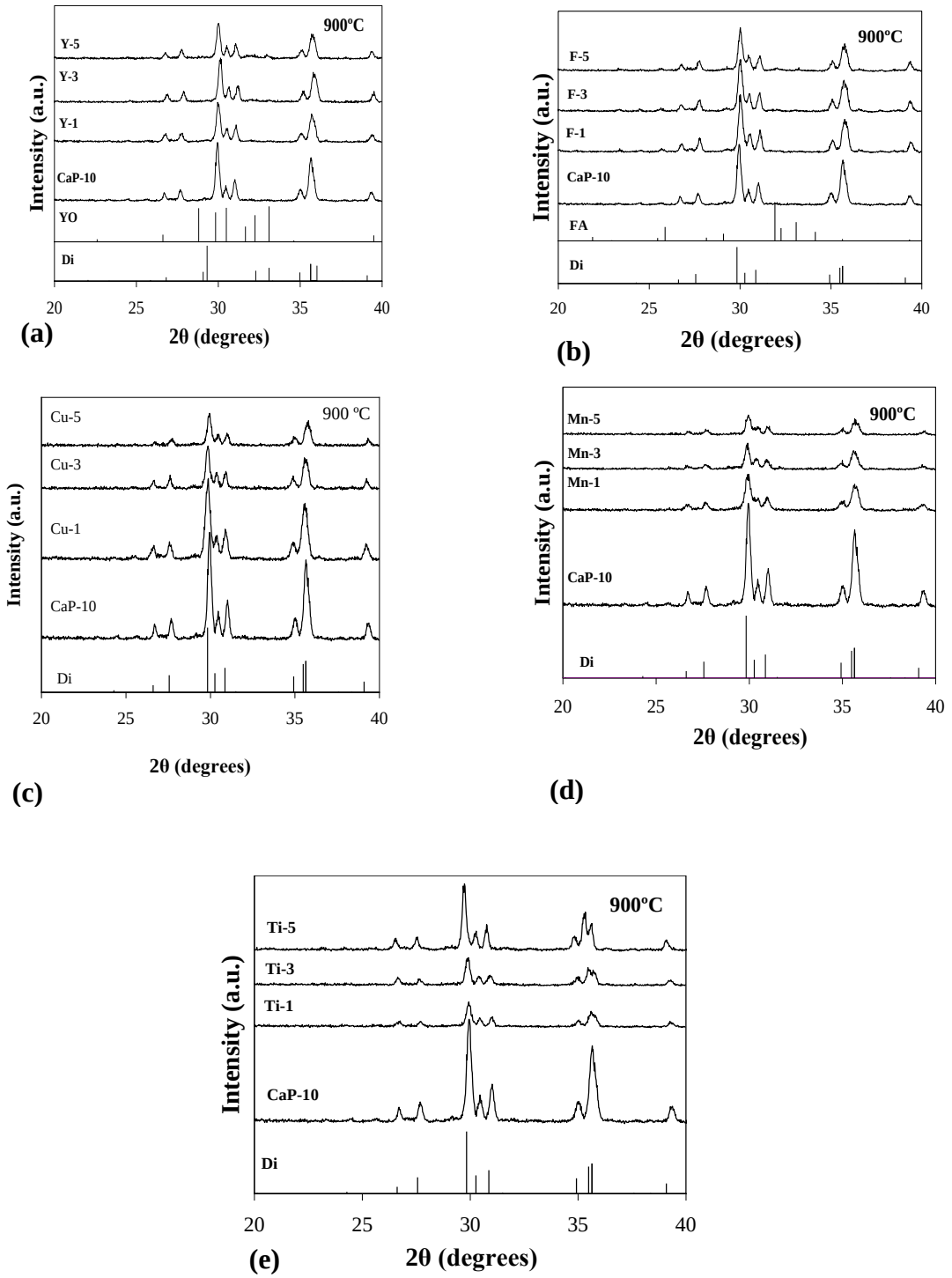

Figure 3.16 X- ray diffractogram of glass powder compacts after sintering at 900 °C for 1 h

However, in order to validate this claim, we need to make quantitative crystalline phase analysis on these glass-ceramics using Rietveld refinement technique because the variation in intensity may also be a result of preferential orientation of crystals in the glass-ceramic powders. Also, the quantitative crystalline phase analysis of these glass-ceramics will allow determining their amorphous/crystalline ratio which will be beneficial in analysing the bioactivity of the glass-ceramics.

3.7 Scanning electron Microscopy (SEM) analysis

With respect to the microstructure of glass-ceramics as observed by SEM, the data is in good agreement with DTA and XRD analysis of the glasses and resultant glass-ceramics, respectively. Fig. 3.17(a) shows examples of some SEM images of glass-ceramics Y-3 (a, b), Cu-3 (c); and Mn-5 (d) after sintering at 900 ºC for 1 h. All of them exhibit densely sintered glass-ceramic structures. This proves the good sintering ability of the starting glass powders reported above.

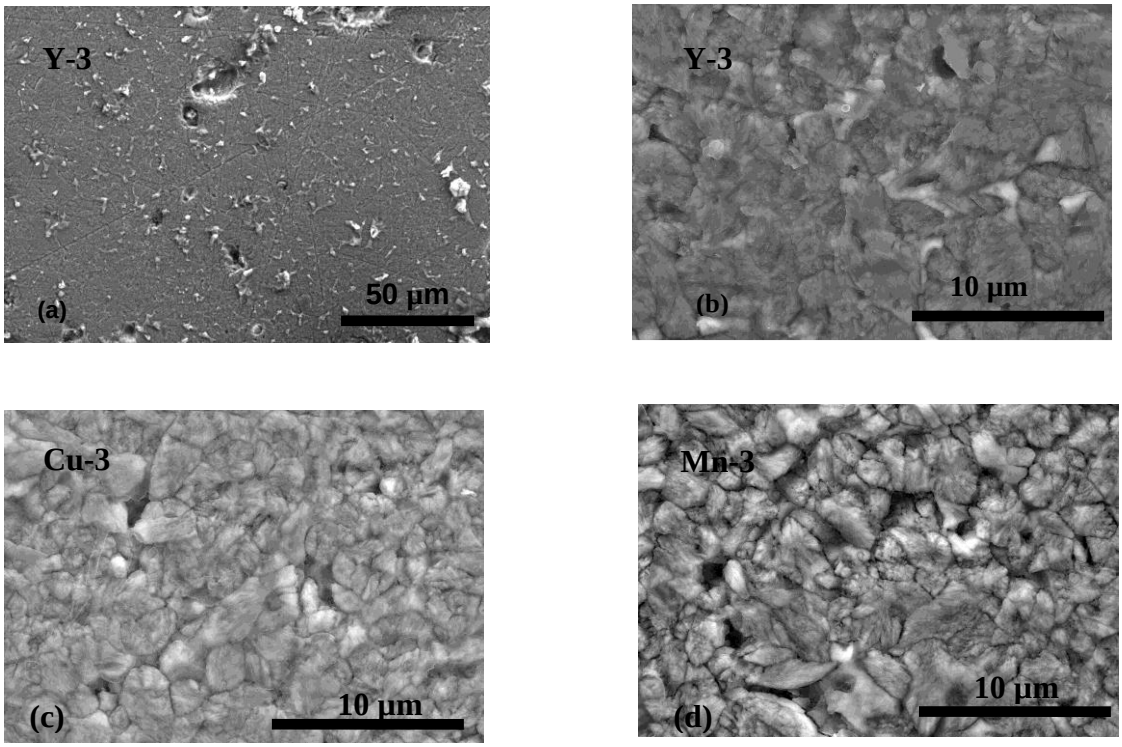

Fig. 3.17 Microstructure (revealed via SEM imaging after chemical etching of polished surfaces with 2 vol.% HF solution) of the glass-ceramic heat treated at 900 °C (a, b) for Y-3; (c) for Cu-3; (d) for Mn-5.

Elemental mapping was also performed for most of the compositions studied to access the homogeneity of the elements distribution and in an attempt to find supporting evidences for the XRD data gathered. Fig. 3.18 shows a SEM microstructure of the F-5 glass ceramic after sintering at 900ºC, as well as the mapping for the most relevant elements in the composition.

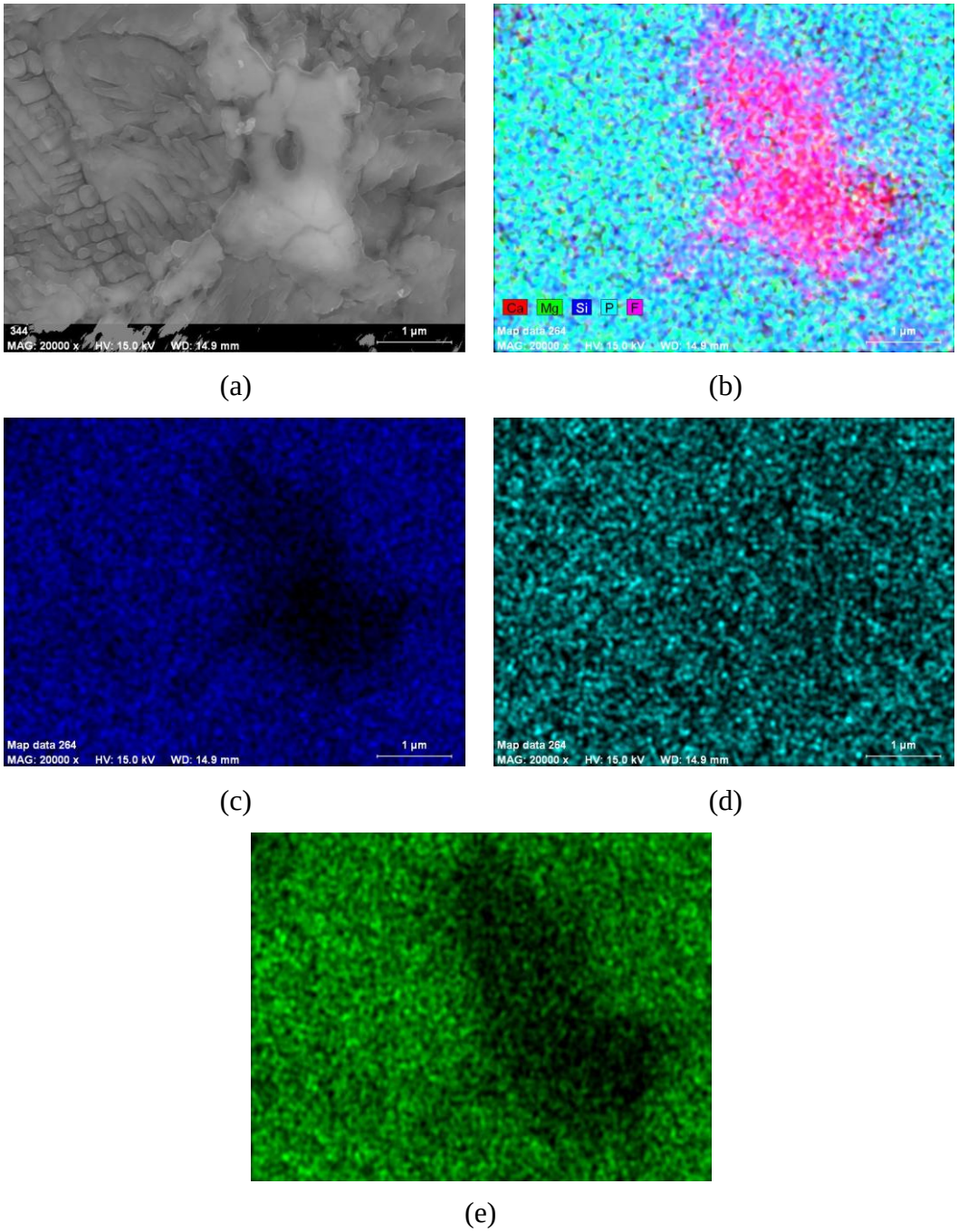

(a) (b)

(c) (d)

(e)

Fig. 3.18 SEM microstructure of sample F-5 heat treated at 900 °C and mapping of the most relevant elements in the composition.

From the elemental mapping, it can be suggested that the main crystal seen in Fig. 3.18 (a) is depleted in Ca, Si and Mg and, therefore, can be attributed to the main crystalline phase (Diopside) detected by XRD. Fig. 3.18 (b) shows that Ca, P and F co-exist in the red-pink spot, together with P. This elemental combination suggests that a segregation phase of a Ca, F, and P elemental combination, as a kind of precursor for fluorapatite has been formed. Its presence can be ascertained by the quite small beak intensity in the XRD spectrum of this sample as shown in Fig. 3.16 (b).

Fig. 3.18 (c) & (e) show that the distribution of Si and Mg elements appear associated, certainly in the main crystalline phase (Diopside) detected by XRD (Fig. 3.16 (b)), as well as in the glassy phase. On the other hand, P appears well distributed in the entire sample, suggesting that besides its involvement in the formation of the fluorapatite precursor, it also exists in the glassy phase as proved by FTIR.

Figure 3.19 shows a SEM microstructure of the Y-5 sample heat treated at 900ºC and the respective elemental mapping. A cluster of Si is well noticed in Fig. 3.19 (b, d), probably corresponding to some remnant from colloidal silica used during final step of polishing. Mg, P and Ca elements appear well combined, probably in the diopside phase [Fig. 3.19 (b)].

This elemental map also suggests some clustering of Y in yttrium Oxide crystalline phase, as detected by XRD fig. 3.16 a. On the other hand, the Y, Mg and P elements appear reasonably well distributed in Fig. 3.19 (c, e and f).

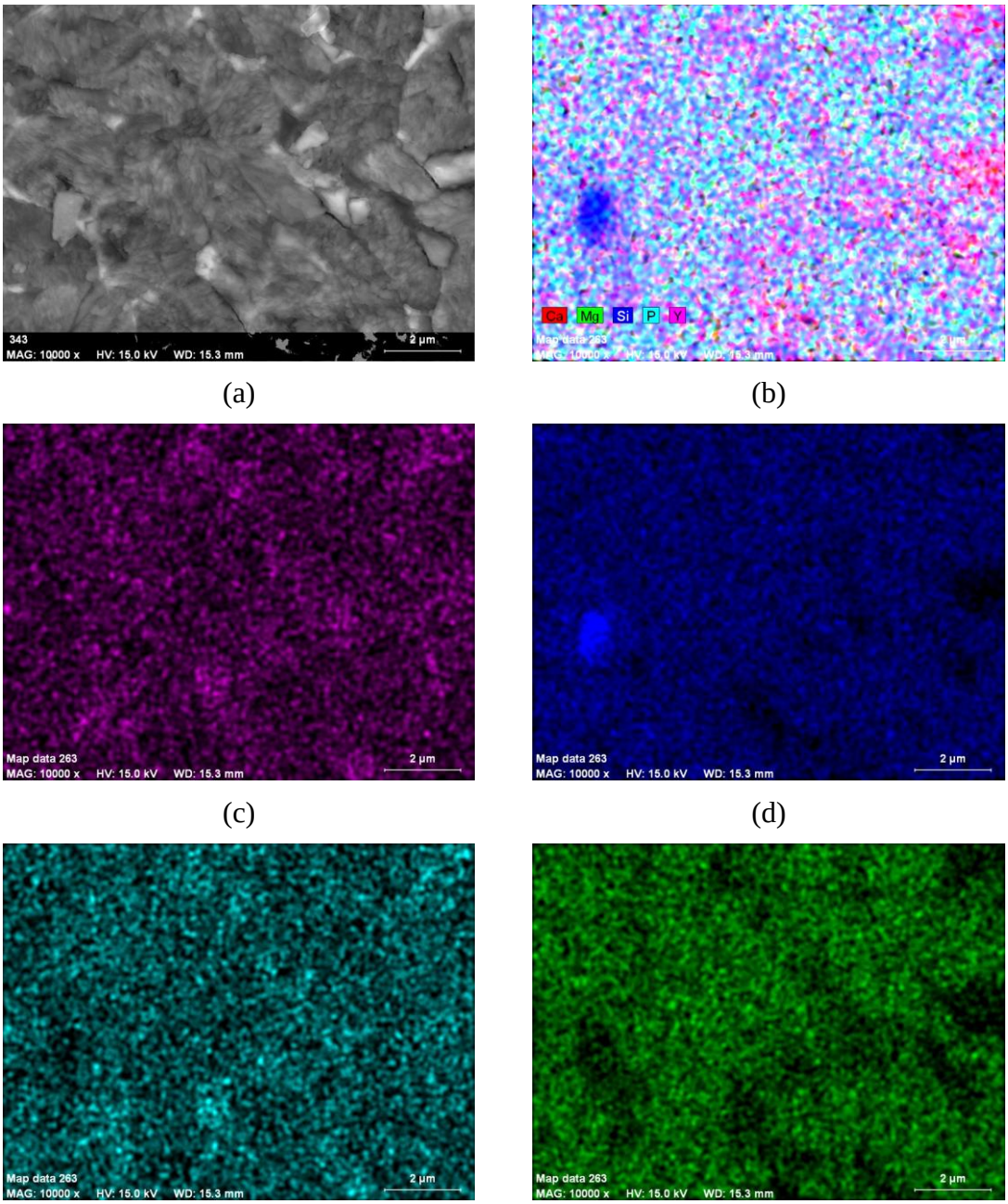

Fig. 3.19 SEM microstructure of sample Y-5 heat treated at 900 °C and mapping of the most relevant elements in the composition.

In summary, the SEM analysis support the experimental results obtained by other characterisation techniques. In other words, the set of results obtained along the present work is consistent, although further work needs to be done to further deepen and confirm same aspects that are not yet enough proven.

Chapter 4
Conclusions

4. Conclusions

The structural characteristics along with the biomineralisation behaviour of a new series of potentially bioactive glasses in Di-CaPP system have been investigated in order to develop a suitable candidate material for biomedical applications. Further, thermal properties and sintering have been discussed as well as the influence of doping various wt. % of Y_2O_3, CaF_2, CuO, MnO, and TiO_2 on various thermo-physical properties of the parent glass. Bioactivity was evaluated by immersion the glass powders SBF for different time periods. No bioactivity test was performed for the bulk glasses and glass ceramics.

From the observations made along the present work, the following conclusions can be drawn:

i) Amorphous and transparent bulk glass could be produced at parent glass from a composition with CaPP $\leq$ 10 wt. %, while above 10 wt. % of CaPP it was not possible to obtain homogeneous transparent glass, since the melts showed a tendency to surface crystallization. Accordingly, almost crystalline and opaque bulk glasses were obtained at 20 wt. %, and 30 wt. % of CaPP, respectively.

ii) Highly homogenous and transparent glasses could be prepared for all the investigated compositions, (except for Ti-5 glass) which showed some traces of crystallinity, suggesting that TiO_2 is playing the role of a nucleating agent.

iii) The incorporation of additives to the parent glass CaP-10 increased the glass density (ρ) irrespective of the nature of additive and led to a gradual decrease in their excess volume while their molar volumes either remained constant or decreased, respectively.

iv) The parent glass and all doped glasses exhibit the dominance of Q^2 (Si) structural units in the glasses, thus implying towards high rate of bioactivity, although a slight depolymerisation has been depicted in all doped glass.

v) The CTE values of almost all the glasses depicted a decrease with initial addition of additives (1 wt. %), before exhibiting an increase with further additions (except for Mn containing glasses).

vi) The T_g values of all doped glasses were evidently lower than their parent glass composition, CaP-10.

vii) The increase in wt. % of Y_2O_3 in the glasses lead to a slight increases on the value of T_g, while increasing wt. % of (CaF_2, CuO, MnO) in the glasses lead to decrease on the values of T_g, while the increase in wt. % of TiO_2 had no significant effect on T_g.

viii) In Yttria-doped glasses, a gradual increase in the values of maximum crystallization peak temperature, T_p, could be observed up to about Y-3, a trend that was reversed with further increasing the amount of doping oxide (Y-5) while an opposite trend was observed in the Ti- doped glasses. These results point out to a first gradual enhancement of the stability of the Y-doped glasses against devitrification, followed a less stability towards crystallisation. The other doped glasses (F-Cu-Mn) exhibited a similar trend, with a gradual decrease in T_p, meaning an increased tendency towards dvitrification.

ix) As deduced from DTA analysis, a large difference between glass transition temperature (T_g) and the onset temperature of crystallization (T_c), ($\Delta T = T_c - T_g$) provides a large processing window that facilitates sintering and ensures thermal stability. According to this criterion, the sintering ability was enhanced with increasing added amounts of yttrium- and fluoride-doped glasses, while the opposite trend has been observed for Cu, Mn, and Ti-doped glasses. However, even in these last cases, the processing window is still enough wide to ensure good sinter ability, as confirmed by SEM imaging.

x) All Y_2O_3, MnO, CuO and TiO_2 containing glasses exhibited a fast biomineralization rate with the formation of a HA layer after 1 h of immersion of the glass powders in a SBF solution, making them good candidates for biomedical applications. Besides HA, silica (SiO_2) and calcium pyrophosphate have been detected on the surface of Mn-5, while calcite together with HA were formed on surface of Y-1and Y-5.

Di crystallized as the main phase in all the glass-ceramics, while a small amount of fluorapatite and calcium silicate were also detected in Fluor-containing glass-ceramics, especially in F-5. In the case of Y-containing glass-ceramics, besides the main Di phase, magnesium yttrium silicate and yttrium oxide were also detected as minor phases. However, Rietveld refinement studies are would be required for a quantitative phase analysis and to get better insight about the distribution of doping elements in the investigated systems.

Future Directions

Regrettably, the shortage of time did not allow a more detailed and in deep study and characterization of the properties of the glasses and glass ceramics prepared in the frame of this Master thesis work programme. Therefore, the following issues are worthy to be continued in a next future:

i) Hot stage microscopy (HSM) analysis must be performed to better understanding the sintering behaviour of glass powders and discrimination between the densification and crystallization phenomena. This will enable gathering further evidences to support our hypothesis of a large sintering temperature window along which the designed glasses can undergo full densification.

ii) Rietveld refinement studies are crucial in order to determine the quantitative phase analysis and get a better insight about the distribution of the doping elements in the investigated systems.

iii) Mechanical strength measurements, including flexural strength, micro-hardness and elastic properties should be measured on the synthesized glasses and glass ceramics.

iv) The physic-chemical degradation of the glasses should be performed in Tris-HCl and citric acid buffer in accordance with ISO 10993-14 and compared with that of bench mark materials existing in the market such as the 45S5 Bioglass®.

v) More exhaustive biomineralization experiments should be carried out by immersing the glass powders and/or bulk glasses or glass ceramics in SBF while registering the evolution of pH and measuring the concentrations of leached ions along the time and performing a more in deep characterization of the deposited HA layer.

vi) Bioactivity experiments in cell or tissue cultures should be conducted using powder/bulk glasses/glass ceramics to study the biological response to designed materials, namely in terms of cell adhesion, cells viability and alkaline phosphatase secretion to evaluate the suitability of the materials for in vivo tests and clinical assays.

References

1. Hench, L.L., et al., *Bioactive ceramics: theory and clinical applications*. Bioceramics Vol. 7-ed. 1994, Oxford, U.K. Butterworth-Heinemann: O.H. Anderson and A. Yli-Urpo.
2. Ioannis, X.D., et al., *Gene-expression profiling of human osteoblasts following treatment with the ionic products of Bioglass® 45S5 dissolution.* J. Of Biomedical Materials Research, 2001. **55**(2): p. 151- 157.
3. Hench, L.L., et al., *Third-Generation Biomedical Materials.* Science, 2002. **295**(1014): p. 1016-1017.
4. Boccaccini, A.R., A.A. Gorustovich, and J.A. Roether . -, *Effect of Bioactive Glasses on Angiogenesis: A Review of In Vitro and In Vivo Evidences.* Tissue Engineering Part B Reviews, 2010. **16** (2): p. 199-207.
5. Hench, L.L., et al., *A genetic basis for biomedical materials. : Its Nucleation and Growth.* Materials Science and Engineering, 2002: p. 283-296.
6. Kansal, I., et al., *Structure, surface reactivity and physico-chemical degradation of fluoride containing phospho-silicate glasses.* Journal of Materials Chemistry, 2011. **21**(22): p. 8074-8084.
7. Hoppe, A., N.S. Güldal, and A.R. Boccaccini, *A review of the biological response to ionic dissolution products from bioactive glasses and glass-ceramics.* Biomaterials, 2011. **32**(11): p. 2757-2774.
8. Meleti, Z., I.M. Shapiro, and C.S. Adams, *Inorganic phosphate induces apoptosis in osteoblast-like cells.* Journal of Dental Research, 2000. **79**: p. 170-170.
9. Murphy, S., et al., . *The effect of ionic dissolution products of Ca-Sr-Na-Zn-Si bioactive glass on in vitro cytocompatibility.* Journal of Materials Science-Materials in Medicine, 2010. **21**(10): p. 2827-2834.
10. Yamaguchi, M., et al., *Role of zinc in bone formation and bone resorption.* The Journal of Trace Elements in Experimental Medicine, 1998. **11**(2-3): p. 119-135.
11. Cacaina, D., et al., *Study of yttrium containing bioactive glasses behaviour in simulated body fluid.* Journal of Materials Science: Materials in Medicine, 2006. **17**(8).
12. Lusvardi, G., et al., *Fluoride-containing bioactive glasses: Surface reactivity in simulated body fluids solutions.* Acta Biomaterialia, 2009. **5**(9): p. 3548-3562.

13. Mulligan, A.M., M. Wilson, and J.C. Knowles., *The effect of increasing copper content in phosphate-based glasses on biofilms of Streptococcus sanguis.* Biomaterials,, 2003. **24**(10): p. 1797-1807.
14. Tilocca, A., et al., *Structural models of bioactive glasses from molecular dynamics simulations.* Proceedings of the Royal Society a-Mathematical Physical and Engineering Sciences, 2009. **465**(2104): p. 1003-1027.
15. Hill, R.G., et al., *Influence of magnesia on the structure and properties of bioactive glasses.* Journal of Non-Crystalline Solids, 2010. **356**(9-10): p. 517-524.
16. Kansal, I., et al., *Structural analysis and thermal behavior of diopside-fluorapatite-wollastonite-based glasses and glass-ceramics.* Acta Biomaterialia, 2010. **6**(11): p. 4380-4388.
17. Linati, L., et al., *Medium-range order in phospho-silicate bioactive glasses: Insights from MAS-NMR spectra, chemical durability experiments and molecular dynamics simulations.* Journal of Non-Crystalline Solids, 2008. **354**(2-9): p. 84-89.
18. Lusvardi, G., et al., *Elucidation of the structural role of fluorine in potentially bioactive glasses by experimental and computational investigation.* Journal of Physical Chemistry B, , 2008. **112**(40): p. 12730-12739.
19. Lusvardi, G., et al., *Quantitative Structure-Property Relationships of Potentially Bioactive Fluoro Phospho-silicate Glasses.* Journal of Physical Chemistry B, 2009. **113**(30): p. 10331-10338.
20. Menziani, M.C., A. Pedone, and G. Malavasi *Computational Insight into the Effect of CaO/MgO Substitution on the Structural Properties of Phospho-Silicate Bioactive Glasses.* Journal of Physical Chemistry C, 2009. **113**(35): p. 15723-15730.
21. Tilocca, A.a.A.N.C., *Structural Effects of Phosphorus Inclusion in Bioactive Silicate Glasses.* The Journal of Physical Chemistry B,2007. **111**(51): p. 14256-14264.
22. Schneider, J., et al., *Si-29 MAS-NMR studies of Q(n) structural units in metasilicate glasses and their nucleating ability.* Journal of Non-Crystalline Solids, 2000. **273**(1-3): p. 8-18.
23. Nonami, T.a.S.T., *Study of diopside ceramics for biomaterials.* Journal of Materials Science-Materials in Medicine, 1999 **10**(8): p. 475-479.

24. Sainz, M.A., et al., *Influence of design on bioactivity of novel CaSiO3-CaMg(SiO3)2 bioceramics: In vitro simulated body fluid test and thermodynamic simulation.* Acta Biomaterialia, 2010. **6**(7): p. 2797-2807.
25. Webster, T.J., et al., *Hydroxylapatite with substituted magnesium, zinc, cadmium, and yttrium. II. Mechanisms of osteoblast adhesion.* Journal of Biomedical Materials Research, 2002. **59**(2): p. 312-317.
26. Sato, M., et al. , *Increased osteoblast functions on undoped and yttrium-doped nanocrystalline hydroxyapatite coatings on titanium.* Biomaterials, 2006. **27**(11): p. 2358-2369.
27. Owada, H., et al., *Humidity-sensitivity of yttrium substituted apatite ceramics.* Solid State Ionics, 1989. **35**(3-4): p. 401-404.
28. Chang, K.A., et al., *Biphasic Electrical Currents Stimulation Promotes both Proliferation and Differentiation of Fetal Neural Stem Cells.* Plos One, 2011. **6**(4).
29. Zhang, J., et al., *Effect of yttrium ion on the proliferation, differentiation and mineralization function of primary mouse osteoblasts in vitro.* Journal of Rare Earths, 2010. **28**(3): p. 466-470.
30. Jamieson, C., K., et al., *Bioactive glasses as potential radioisotope vectors for in situ cancer therapy: investigating the structural effects of yttrium.* . Phys. Chem. , 2001. **13**: p. 17749-17755.
31. Wiegand, A., W. Buchalla, and T. Attin, *Review on fluoride-releasing restorative materials-Fluoride release and uptake characteristics, antibacterial activity and influence on caries formation.* Dental Materials, 2007. **23**(3): p. 343-362.
32. Aaseth, J., et al. , *Fluoride: A toxic or therapeutic agent in the treatment of osteoporosis?* The Journal of Trace Elements in Experimental Medicine, 2004 **17**(2): p. 83-92.
33. Vestergaard, P., et al., *Effects of treatment with fluoride on bone mineral density and fracture risk - a meta-analysis.* Osteoporosis International, 2008. **19**(3): p. 257-268.
34. Pak, C.Y.C., J.E. Zerwekh, and P. Antich, *Anabolic effects of fluoride on boneTrends in Endocrinology &amp.* Metabolism, 1995. **6**(7): p. 229-234.
35. Gérard, C., et al., *The stimulation of angiogenesis and collagen deposition by copper.* Biomaterials, 2010. **31**(5): p. 824-831.

36. Dahl, S.L.M., R.B. Rucker, and L.E. Niklason, *Effects of copper and cross-linking on the extracellular matrix of tissue-engineered arteries.* Cell Transplantation, 2005. **14**(6): p. 367-374.
37. Pablo, J.R., et al., *Modulation of the Proliferation and Differentiation of Human Mesenchymal Stem Cells by Copper.* Journal of Cellular Biochemistry, 2002. **85**: p. 92-100.
38. Culotta, V.C., M. Yang, and M.D. Hall, *Manganese Transport and Trafficking: Lessons Learned from Saccharomyces cerevisiae.* Eukaryotic Cell, 2005. **4**(7): p. 1159-1165.
39. Mould, A.P., S.K. Akiyama, and M.J. Humphries, *Regulation of Integrin α5β1-Fibronectin Interactions by Divalent Cations.* Journal of Biological Chemistry, 1995. **270**(44): p. 26270-26277.
40. Medvecký, Ľ., et al., *Influence of manganese on stability and particle growth of hydroxyapatite in simulated body fluid.* Colloids and Surfaces A: Physicochemical and Engineering Aspects, 2006. **281**(1-3): p. 221-229.
41. Rico, H., et al., *Effects on bone loss of manganese alone or with copper supplement in ovariectomized rats: A morphometric and densitomeric study.* European Journal of Obstetrics & Gynecology and Reproductive Biology, 2000. **90**(1): p. 97-101.
42. Lüthen, F., et al., *Influence of manganese ions on cellular behavior of human osteoblasts in vitro.* Biomolecular Engineering, 2007. **24**(5): p. 531-536.
43. Guangda, L., et al., *Magnetic bioactive glass ceramic in the system CaO-P2O5-SiO2-MgO-CaF2-MnO2-Fe2O3 for hyperthermia treatment of bone tumor.* J Mater Sci. Mater Med, 2011. **22**: p. 2197-2206.
44. Saiz, E., et al., *Characterization of Metal/Glass Interfaces in Bioactive Glass Coatings on Ti-6Al-4V and Co-Cr Alloys, in Nano and Microstructural Design of Advanced Materials.* Elsevier Science Ltd: Oxford, 2003: p. 61-67.
45. Vrouwenvelder, W.C.A., C.G. Groot, and K. de Groot, *Better histology and biochemistry for osteoblasts cultured on titanium-doped bioactive glass: Bioglass 45S5 compared with iron-, titanium-, fluorine- and boron-containing bioactive glasses.* Biomaterials, 1994. **15**(2): p. 97-106.

46. Abou Neel, E.A., et al., *In vitro bioactivity and gene expression by cells cultured on titanium dioxide doped phosphate-based glasses.* Biomaterials, 2007. **28**(19): p. 2967-2977.
47. Tas, A.C., *Synthesis of Biomimetic Ca-Hydroxyapalite Powders at 37 °C in synthetic body fluids.* Biomaterials, 2000. **21**: p. 1429-38.
48. Kokubo T., T.H., *How useful is SBF in predicting in vivo bone bioactivity.* Biomaterials, 2006. **27**: p. 2907-15.
49. Komatsu, T., et al., *Quenched-in excess volume and structural relaxation in Ni-and Fe-Ni based metallic glasses.* J. Of non- crystalline solids, 1986. **3**(2.): p. 358-374.
50. Lacerda, S.R., et al., *TiO_2-introduced phase separation and crystallization in SiO_2-3CaO. P_2O_5-MgO glass.* J. of non crystalline solids, 1997. **221**: p. 255-260.
51. Silva, A.M., et al., *Structure and degradation behaviour of Calcium phosphate glasses.* Mat. Sci. And eng., 2011. **18**: p. 192021.
52. Vitor, M.F., Marques, et al., *The effect of TiO2 and P2O5 on densification behavior and properties of Anortite-Diopside glass-ceramic substrates.* J Electroceram. , 2010. **25**: p. 38-44.
53. Abo-Mosallam, H.A., et al., *MAS-NMR studies of glasses and glass-ceramics on a clinopyroxene-fluorapatite system.* J. Mater. Chem., 2010. **20**: p. 790-797.
54. Antonio, A., et al., *The origin of nanostructuring in potassium niobiosilicate glasses by Raman and FTIR spectroscopy.* J. Non-Cryst. Solids, 2005. **351**: p. 3610-3618.
55. Lucovsky, L.G.a.G., *Longitudinal Optical Vibrations in Glasses:GeO_2 and SiO_2.* Phys. Rev. Lett., 1976. **37**: p. 1474.
56. Lockyer, M.W.G., et al., *NMR investigation of the structure of some bioactive and related glasses.* Journal of non-Crystalline Solids, 1995. **88**: p. 207-219.
57. Delia, S.B., et al., *Structure of fluoride-containing bioactive glasses.* J. Mater. Chem., 2009. **19**: p. 5629- 5636.
58. Tilocca, A., et al., *Structure and dynamics of bioactive phosphosilicate glasses and melts from ab initio molecular dynamics simulations.* Phys. Rev. B, 2007. **76**: p. 224202.
59. Shih, P.Y., et al., *^{31}P Mas-NMR and FTIR analyses on the structure of CuO-containing poly-and meta-phosphate glasses.* Mat. Chemist. And physic. , 2003. **80**: p. 391-396.

60. Zotov, N., et al., *Effect of MnO-doping on the structure of sodium metaphosphate glasses.* Z. Naturforsch, 2003. **58a**: p. 419-428.
61. Hess., M.I.W.a.P.C., *The Structural Role of $A1_2O_3$ and TiO_2 in Immiscible silicate liquids in the system SiO_2 -MgO- CaO-FeO-TiO_2 -AI_2O_3.* Contrib. Mineral. Petrol. , 1980. **72**: p. 319-328 .
62. Virgo, B.O.M.a.D., *The solubility behavior of CO_2 in melts on the join $NaAlSi_3O_8$-$CaAl2Si_2O_8$ at high pressure and temperature: a Raman spectroscopic study.* American Mineralogist, 1980. **65**: p. 1166-1175.
63. Wren, A.W., et al., *The bioactivity and ion release of titanium-containing glass polyalkenoate cements for medical applications.* J Mater Sci: Mater Med., 2011. **22**: p. 19-28.
64. Robert G. Hill, e.a., *Predicting the glass transition temperature of bioactive glasses from their molecular chemical composition.* Acta Biomaterialia, 2011. **7**: p. 3601-3605.
65. Ray, N.H., *Composition-property relationships in organic oxide glasses.* J. Of non-crystalline solids, 1974. **15**(3): p. 423-434.
66. Costantini, A., et al., *Effect of the substitution of Y2O3 for CaO on the bioactivity of 2.5 CaO-2SiO2 glass.* Biomaterials, 1997. **18**: p. 453-458.
67. Wu, L., et al., *Electrochemical performance of Ti -doped $LiFePO_4$ synthesized by co-precipitation and post-sintering method.* Trans. Nonfcrrous Mcl. Soc. China, 2010. **20**: p. 814-818.
68. Cerruti, M.a.C.M., *Carbonate formation on bioactive glasses.* Langmuir, 2004. **20**(15): p. 6382-6388.
69. Hench, L.L., et al., *Bioceramics.* Journal of the American Ceramic Society, 1998. **81**(7): p. 1705-1728.
70. Brauer, D.S., et al., *Fluoride-containing bioactive glasses: Effect of glass design and structure on degradation, pH and apatite formation in simulated body fluid.* Acta Biomaterialia, 2010. **6**(8): p. 3275-3282.
71. Jonathan, L., et al., *New strontium-based boactive glasses: physicochemical reactivity and delivering capability active dissolution products.* Journal of Mar. chemist. , 2009. **19**: p. 2940-2949.

72. Cacaina, D., et al., *The behaviour of selected yttrium containing bioactive glass microspheres in simulated body environments.* J. Mater. Sci. Mater. Med., 2008. **19**: p. 1225-1233.
73. Y. EBISAWA, e.a., *Bioactivity of CaO. SiO2- based glasses: in vitro evalution.* J. Of mat. Sci.: Material in medicine, 1990. **1**: p. 239-244.
74. Takadamam, H., et al., *XPS study of the process of apatite formation on bioactivity Ti-6Al-4V alloy in simulated body fluid.Sci. and Tech.* J. of adv. Mat. , 2001. **2**: p. 389-396.
75. Tadashi, K., et al., *Novel bioactive materials with different mechanical properties.* j of Biomaterials, 2003. **24**: p. 2161-2175. .